International Journal of Applied Earth Observation and Geoinformation 14 (2012) 112–128

Contents lists available at SciVerse ScienceDirect

International Journal of Applied Earth Observation and Geoinformation

journal homepage: www.elsevier.com/locate/jag

Review

Multi- and hyperspectral geologic remote sensing: A review

Freek D. van der Meer*, Harald M.A. van der Werff, Frank J.A. van Ruitenbeek, Chris A. Hecker, Wim H. Bakker, Marleen F. Noomen, Mark van der Meijde, E. John M. Carranza, J. Boudewijn de Smeth, Tsehaie Woldai

University of Twente, Faculty of Geo-information Science and Earth Observation (ITC), Hengelosestraat 99, 7514 AE Enschede, The Netherlands

ARTICLE INFO

Article history:
Received 24 December 2010
Accepted 10 August 2011

Keywords:
Geologic remote sensing
Landsat
ASTER
Hyperspectral

ABSTRACT

Geologists have used remote sensing data since the advent of the technology for regional mapping, structural interpretation and to aid in prospecting for ores and hydrocarbons. This paper provides a review of multispectral and hyperspectral remote sensing data, products and applications in geology. During the early days of Landsat Multispectral scanner and Thematic Mapper, geologists developed band ratio techniques and selective principal component analysis to produce iron oxide and hydroxyl images that could be related to hydrothermal alteration. The advent of the Advanced Spaceborne Thermal Emission and Reflectance Radiometer (ASTER) with six channels in the shortwave infrared and five channels in the thermal region allowed to produce qualitative surface mineral maps of clay minerals (kaolinite, illite), sulfate minerals (alunite), carbonate minerals (calcite, dolomite), iron oxides (hematite, goethite), and silica (quartz) which allowed to map alteration facies (propylitic, argillic etc.). The step toward quantitative and validated (subpixel) surface mineralogic mapping was made with the advent of high spectral resolution hyperspectral remote sensing. This led to a wealth of techniques to match image pixel spectra to library and field spectra and to unravel mixed pixel spectra to pure endmember spectra to derive subpixel surface compositional information. These products have found their way to the mining industry and are to a lesser extent taken up by the oil and gas sector. The main threat for geologic remote sensing lies in the lack of (satellite) data continuity. There is however a unique opportunity to develop standardized protocols leading to validated and reproducible products from satellite remote sensing for the geology community. By focusing on geologic mapping products such as mineral and lithologic maps, geochemistry, P-T paths, fluid pathways etc. the geologic remote sensing community can bridge the gap with the geosciences community. Increasingly workflows should be multidisciplinary and remote sensing data should be integrated with field observations and subsurface geophysical data to monitor and understand geologic processes.

Contents

* Corresponding author. Tel.: +31534874353; fax: +31534874336.
E-mail address: vdmeer@itc.nl (F.D. van der Meer).

0303-2434/$ – see front matter © 2011 Elsevier B.V. All rights reserved.
doi:10.1016/j.jag.2011.08.002

1. Introduction

Geological remote sensing has been ill-defined in the literature. The name suggests that remote sensing data (this can be field-based, airborne or spaceborne geophysical measurements) are used to study geology. Traditionally, geology deals with the composition, structure, and history of the Earth. However, more and more geology deals with processes that have formed the Earth and other planets indicating that geology becomes more multidisciplinary and more positioned on issues of societal relevance. There are several text books on geologic remote sensing. However, these books predominantly are introductory to remote sensing using examples in the field of geosciences. Floyd Sabins wrote probably one of the most sold and cited textbooks on remote sensing (Sabins, 1996). Although he is a remote sensing geologist, his book is written for the general remote sensing audience contrary to the book of Steven Drury, another remote sensing geologist, who dedicated a book to geologic image interpretation (Drury, 1987). Ravi Gupta, professor from the Earth Sciences department of the University of Roorkee (India) wrote a book on geologic remote sensing (Gupta, 2003). In addition, there are a number of review articles on aspects of geologic remote sensing including remote sensing for mineral exploration (Sabins, 1999), applications of hyperspectral remote sensing in geology (Cloutis, 1996), and the use of remote sensing and GIS in mineral resource mapping (Rajesh, 2004). Some of the early founding papers were published by Gregg Vane and Alexander Goetz when both were working at the NASA Jet Propulsion Laboratory (Vane and Goetz, 1993, 1988). Much of the geologic remote sensing in the visible-near infrared (VNIR), shortwave infrared (SWIR), mid infrared (MIR) and thermal infrared (TIR) part of the spectrum resulted from pioneering work of Hunt and Salisbury (Hunt, 1977; Salisbury et al., 1989; Cooper et al., 2002) who meticulously measured mineral and rock spectra forming the basis for airborne and spaceborne instruments. Remote sensing geologists have actively contributed to the development of active sensor technology (predominantly SAR and InSAR) and passive sensor technology (multispectral and hyperspectral remote sensing in the VNIR to SWIR and TIR parts of the spectrum). The latter is the subject of this review. The aim is to present an overview of nearly 30 years of science at the interface of geology and remote sensing. This paper is written to take stock of the developments, review the papers that made an impact, signal trends and present some of the shortcomings and future challenges.

Throughout this paper, examples from the Rodalquilar gold mining area (Fig. 1) located in the Sierra del Cabo de Gata (Cabo de Gata National Park) in the south-eastern corner of Spain (Rytuba et al., 1990) will be presented as illustrative products generated from various multi- and hyperspectral sensors using analytical techniques discussed in the text. The area consists of calc-alkaline volcanic rocks (andesites and rhyolites) of late Tertiary age which have been extensively altered to form an assemblage of metamorphic minerals from high to low temperature as: silica, alunite, kaolinite, montmorillonite and chlorite. The following alteration facies (Fig. 2) are distinguished: silicic, advanced argillic, intermediate argillic and propylitic. Associated are high sulfidation gold deposits located in the central part of the volcanic field. The geology, geochemistry and mineralization of the area is well described (Arribas et al., 1995) and several geologic remote sensing studies have been conducted at Rodalquilar (Debba et al., 2009; Bedini et al., 2009; van der Meer, 2006b); hence, it serves as a good example to illustrate various techniques and sensor data sets. The image data used are shown in Fig. 3.

2. Multispectral: the Landsat era

Ratioing techniques and geologic image interpretation date back to the early days of air photo geology and the early Landsat multispectral scanner (MSS) data sets where the VNIR bands were first deployed to derive iron oxide ratio images (Goetz and Rowan, 1981). The French Satellite Pour l'Observation de la Terre (SPOT) system was used by the geology community because of its (at that time) unprecedented spatial resolution and stereo capability. Several studies show the use of SPOT data for lithologic mapping (Bilotti et al., 2000) and for (semi)automatic detection and delineation of faults (Kaya et al., 2004; Kavak, 2005; Kavak and Inan, 2002). It has also been shown that subpixel measurement of surface displacement along faults can be derived from SPOT data (Crippen et al., 1991, 1996). While other instruments such as IRS-1A (Bhan et al., 1991) were also used by the geologic remote sensing community, the uptake of remote sensing in geology accelerated with the advent of the Landsat Thematic Mapper (TM) instrument. Landsat TM images have been used for many years by the geologic remote sensing community for mapping of lithology and delineation of lineaments specifically to map alteration mineralogy. In particular band ratioing techniques, decorrelation stretching and saturation enhancement and principal component (PC) analysis (PCA) have been popular techniques (Chavez et al., 1991; Yesou et al., 1993). The Landsat TM band 7/band 5 ratio is generally used to separate argillic from non-argillic materials, thus, reflecting the presence or absence of hydroxyl absorption bands. Fe-O versus non-Fe-O mapping is done using the band 3/band 1 ratio. A qualitative interpretation scheme for a false color composite ratio image of R = 5/7, G = 3/1, B = 5 in red–green–blue is provided in Table 1. Instead of using ratio images, spectral gradients can be used where the gradient expressed as a fraction of the average radiance is given by the intensity of two channels normalized to their average value as (Gillespie et al., 1987):

$$DDN_{ij} = \left(\frac{DN_i - DN_j}{DN_i + DN_j}\right)\frac{2}{\lambda_i - \lambda_j}, \quad (1)$$

where DDN_{ij} is the value of the normalized intensity for Landsat channels i and j and λ_i and λ_j are their respective wavelengths. This normalization reduces the effect of albedo and topographic effects. A qualitative interpretation scheme for a false color composite normalized (following equation (1)) ratio image of 5/7, 3/1, 5 in red–green–blue is provided in Table 2.

To optimally display Landsat (MSS and TM) data in three color composite images, the optimum index factor (OIF) has for some time been used (Chavez et al., 1980). The OIF is calculated for all possible three-band combinations as the ratio of the sum of standard deviations over the sum of correlations. The idea behind this ratio is that the three-band combination that ranks highest on this score theoretically combines the largest amount of 'information' (i.e. a high sum of standard deviations) with the least amount of 'duplication' (i.e. low interband correlation). There are many examples of studies that used the OIF technique to enhance geologic features in

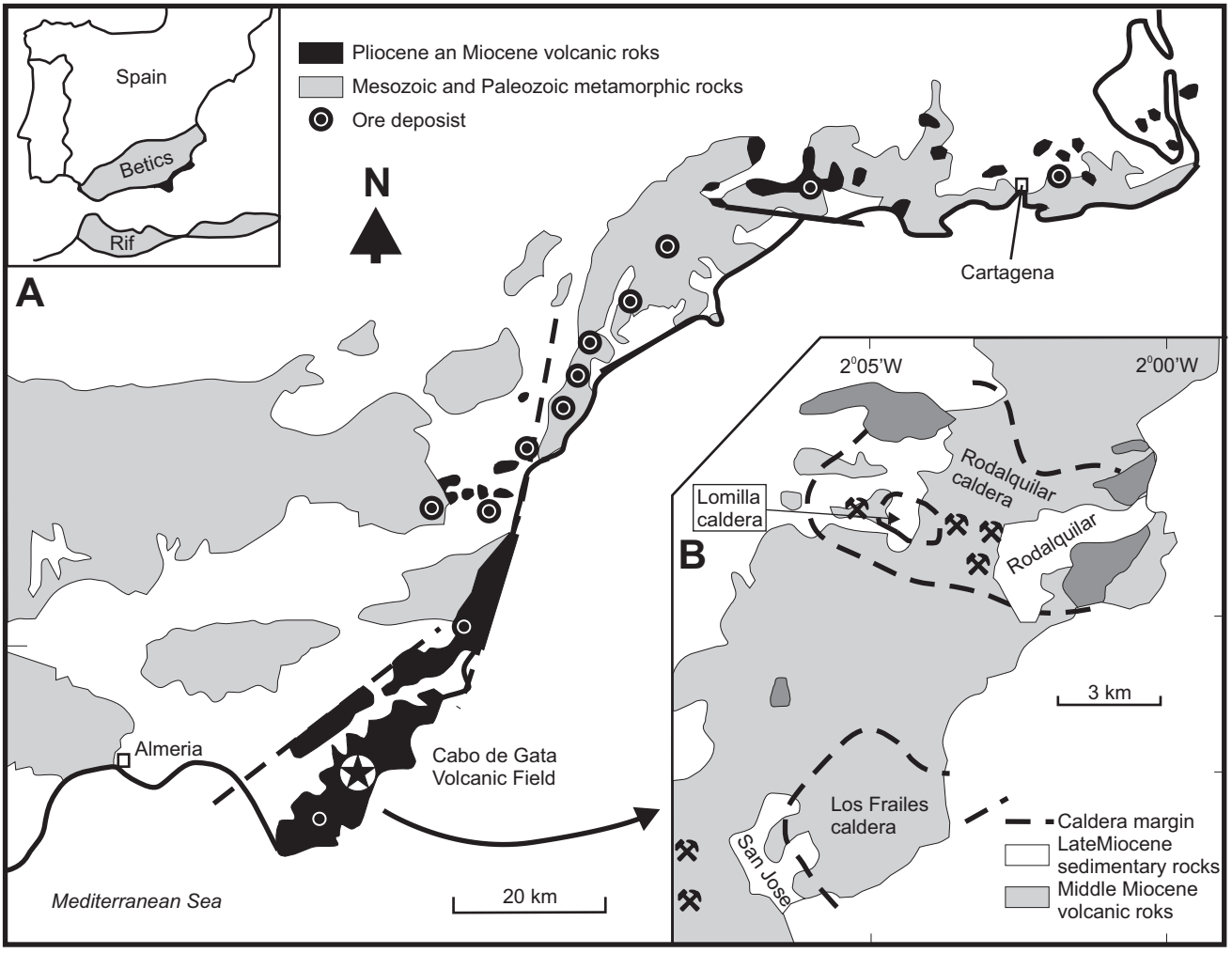

Fig. 1. Location of the Rodalquilar gold deposit (inset map B) in volcanic belt of SE Spain (map A).
Source: Modified after Rytuba et al. (1990).

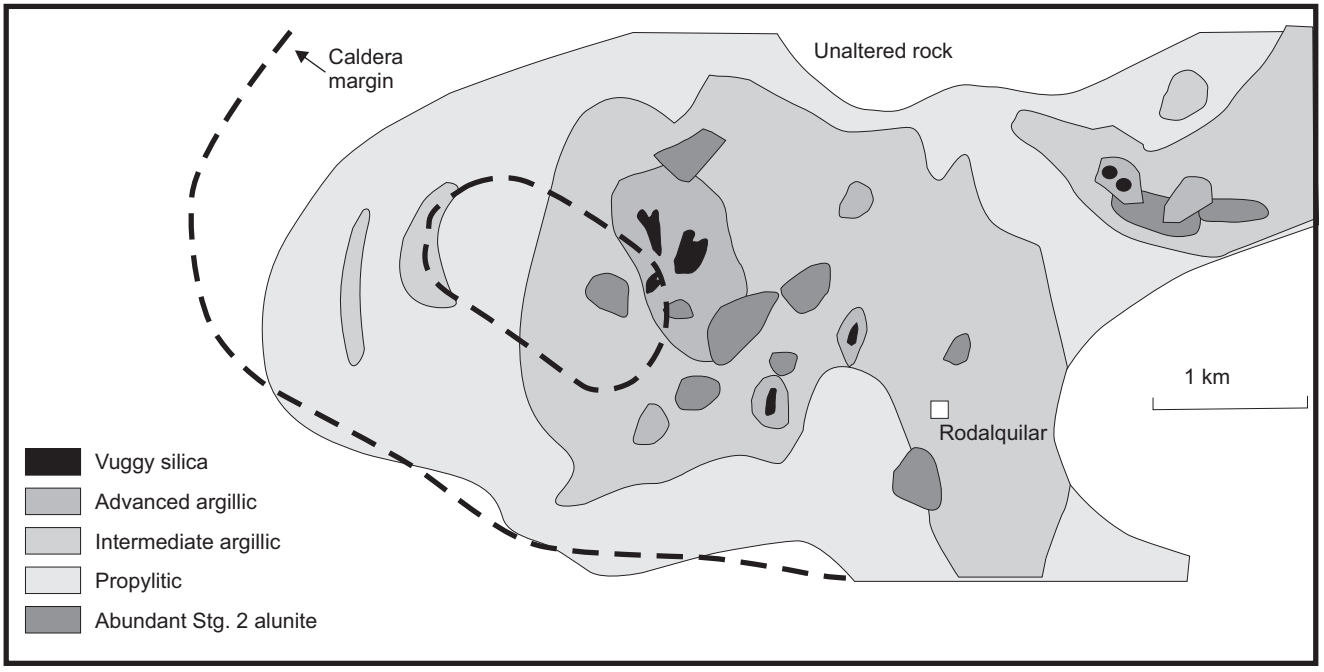

Fig. 2. Simplified surface alteration system of the Rodalquilar caldera (area B in Fig. 1).
Source: Modified after Rytuba et al. (1990).

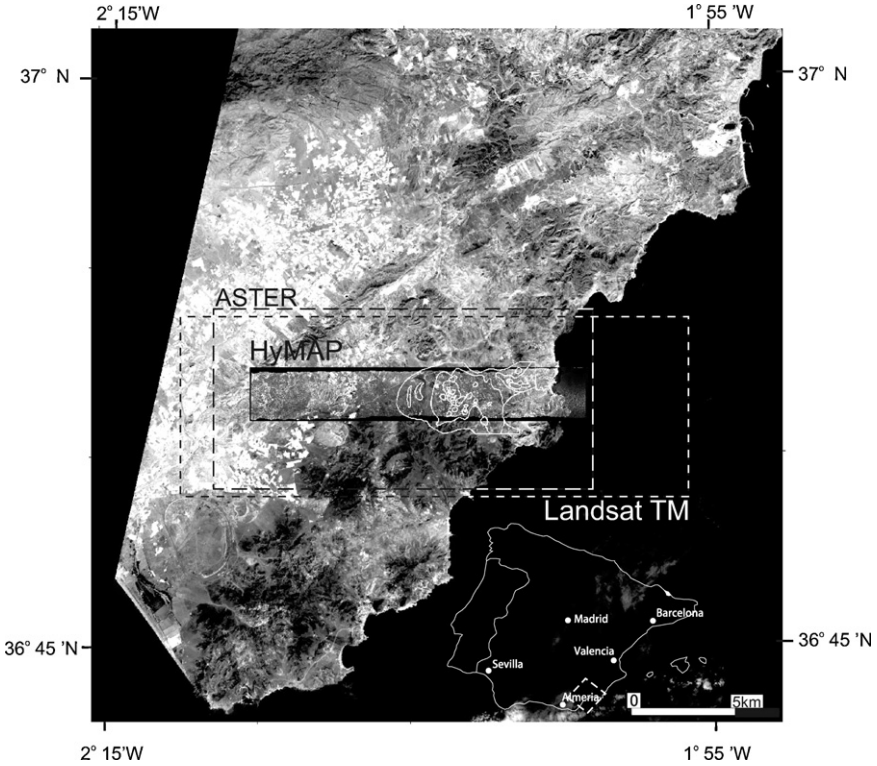

Fig. 3. ASTER image with overlain HyMAP 126 channel imaging spectrometer airborne data set and Landsat TM window used in this study. The alteration system can be depicted on the HyMAP image.

Landsat data (Abrams et al., 1983; Prinz, 1996) and more recently on ASTER data (Gad and Kusky, 2007).

Through the analysis of eigenvalues of PC images spectral information was used to enhance surface mineralogy (Crosta and McMoore, 1989). The technique deployed was coined to the originator, thus the term 'Crosta technique' is often used. Several researchers applied the Crosta method of selective PC analysis for mapping of granitoids (Kalelioglu et al., 2009; Aydal et al., 2007)

Table 1
A qualitative interpretation scheme for a false color composite ratio image of 5/7, 3/1, 5 in red–green–blue.

TM ratio[a]			Image color	Absorption feature
Red:5/7	Green:3/1	Blue:5		
H	L	L	Red	H_2O, OH, low albedo
H	L	H	Magenta	H_2O, high albedo
H	L	M	Pink	H_2O, OH
L	M	L	Dark green	Weak Fe^{3+}, low albedo
L	M–H	L–M	Light green	Weak Fe^{3+}, low albedo, H_2O, OH, carbonaceous materials
L	M–H	M–H	Cyan	Strong Fe^{3+}, moderate albedo, low H_2O
L	L	M	Blue	Moderate albedo
L	M	H	Light blue	High albedo, moderate Fe^{3+}, low H_2O
M–H	M–H	L–M	Yellow	Moderate Fe^{3+}, moderate H_2O
M	M	L	Brown	
H	H	H	White	
L	L	L	Black	

[a] Relative ratio values: L = low; M = moderate; H = high.

Table 2
A qualitative interpretation scheme for a false color composite normalized (according to equation (1)) ratio image of 5/7, 3/1, 5 in red–green–blue.

TM ratio[a]			Image color	Absorption feature
Red:5/7 (normalized)	Green:3/1 (normalized)	Blue:5 (normalized)		
M	L	M	Magenta	H_2O
H	M–H	L	Yellow	Weak H_2O, OH, Fe^{3+}
L	M	L	Dark green	Fe^{3+}
H	L	L	Red	H_2O
L	M–H	M–H	Cyan	Fe^{3+}
L	L–M	M	Dark cyan	Low Fe^{3+}
M–H	L–M	L	Brown	Low Fe^{3+}, moderate H_2O
H	H	H	White	

[a] Relative ratio values: L = low; M = moderate; H = high.

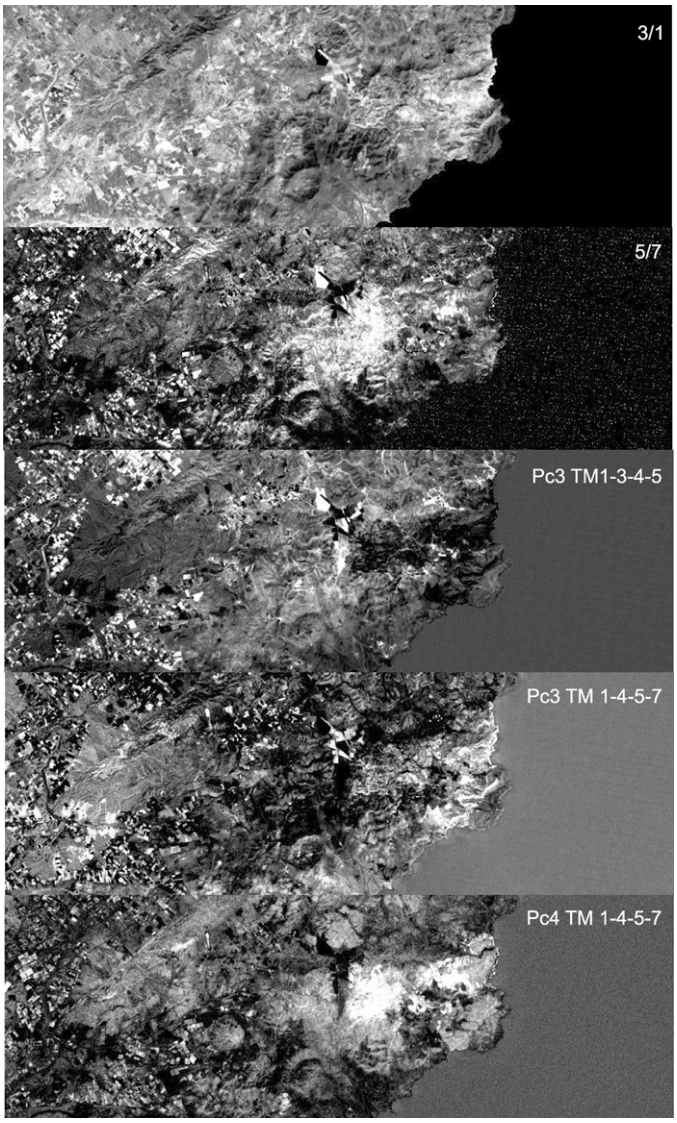

Fig. 4. Examples of Landsat TM geologic products (from top to bottom): 3/1 band ratio, 5/7 band ratio, PC 3 of TM 1-3-4-5, PC 3 of TM 1-4-5-7, PC4 of TM 1-4-5-7.

and alteration systems (Tangestani and Moore, 2001; Ranjbar et al., 2004).

Selective PC analysis using two spectral bands has resulted in ferric iron images (using PC2 on Landsat TM band 1 and 3) and hydroxyl images (using PC2 on Landsat TM band 5 and 7 (Chavez and Kwarteng, 1989). An alternative approach to the use of selective PC analysis on Landsat TM data was the 'feature-oriented PCs' (Loughlin, 1991). Here a hydroxyl image is generated using PC3 or 4 from a Landsat TM 1-4-5-7 band combination and a ferric oxide image is derived from PC4 of a TM 1-3-4-5 band set. Examples of Landsat TM geologic data products for the Rodalquilar site are shown in Fig. 4.

Most geologic remote sensing studies focus on arid environments thus circumventing the problems with outcrops being obscured by the presence of vegetation. A method referred to as the "forced invariance" approach has been proposed to subdue the expression of vegetation and enhance the expression of the underlying lithology in remotely sensed imagery (Crippen and Blom, 2001). The method subsequently corrects for additive path radiance, finds a relationship between a vegetation index and digital number (DN) values in each band, and multiplies the DN values as a function of the index so that the average value becomes invariant across all index values.

Landsat TM data have been used widely by the geologic remote sensing community for a wide range of applications including geologic (Schetselaar et al., 2000; Fraser et al., 1997), lithologic (Gad and Kusky, 2006) and structural (Boccaletti et al., 1998; Yesou et al., 1993) mapping, volcanic deposits and volcano monitoring (Oppenheimer et al., 1993), coral reef mapping (Mumby et al., 1997), natural oil seep detection (Macdonald et al., 1993), landslide mapping (Singhroy et al., 1998; Lee and Talib, 2005) and issues related to mineral exploration (Abdelsalam et al., 2000; Sabins, 1999; Ferrier et al., 2002). Landsat TM data have also been integrated with other airborne geophysical (gravity, magnetic, gamma ray) and spaceborne remote sensing (SAR, SIR-C) data to foster spatially integrated mapping approaches (Kettles et al., 2000) and image fusion techniques such as the IHS transformation have been used widely (Yesou et al., 1993; Rigol and Chica-Olmo, 1998) although it is questionable what the added value in terms of extra information is of a fused product as opposed to the individual products (van der Meer, 1997). Another recent study on physicochemical properties of post mining lakes demonstrated the use of multitemporal analysis Landsat TM5/ETM+7 satellite data as the basis of a monitoring system for the geochemistry of mining lakes (Schroeter and Glasser, 2011; Glasser et al., 2011). An overview of image fusion techniques and applications is provided in (Pohl and van Genderen, 1998).

3. Multispectral: the ASTER era

During recent years, the Advanced Spaceborne Thermal Emission and Reflectance Radiometer, ASTER (Abrams, 2000; Yamaguchi et al., 1998; Abrams and Hook, 1995), on the Terra platform launched on December 18, 1999 has provided enhanced mineral mapping capabilities for the geologic remote sensing community. ASTER (see Table 3 for a programmetric description) is designed with three bands in the VNIR spectral range with a 15 m spatial resolution, six bands in the SWIR with a 30 m spatial resolution, and five bands in the TIR with a 90 m spatial resolution. Simultaneously, a single band in the near-infrared is provided for along-track stereo capability. The swath width is 60 km and the temporal resolution is <16 days. Higher level calibrated ASTER products (radiance, reflectance, emissivity, temperature) can be ordered directly. Unfortunately, ASTER does not have a band in the blue wavelength which Landsat TM has. Thus ASTER cannot produce natural color composite images. However, ASTER has stereo capability allowing the generation of DEM's and the bands in the SWIR allow a wealth of mineral indices to be calculated. In particular the narrow bands in the SWIR and the additional channels in the TIR allow the step from mapping alteration indices (with Landsat TM) to mapping mineral indices. The in situ calibrated ASTER images may be affected by the 'crosstalk' instrument problem, which is caused by light reflected from band 4 optical components leaking into the other SWIR band detectors (Abrams, 2002, personal communication). Particularly band 5 (centred at 2.165 μm) and band 9 (centred at 2.390 μm), physically situated on either side of the band 4 detector on the ASTER instrument, are affected by the anomalous reflectance. Although the anomalous reflectance appears to be small compared to the spectral reflectance differences of typical targets, we believe that the sensor acquires inaccurate reflectance and interpretation in terms of band absorptions is not feasible. ASTER processing and calibration includes channel co-registration, geometric and radiometric correction, crosstalk correction and atmospheric correction, respectively, to retrieve pseudo reflectance data.

Table 3
ASTER band passes and instrument characteristics.

Characteristic	VNIR	SWIR	TIR
Spectral range	1[a]: 0.52–0.60 μm Nadir looking 2: 0.63–0.69 μm Nadir looking 3N: 0.76–0.86 μm Nadir looking 3B: 0.76–0.86 μm Backward looking	4:1.600–1.700 μm 5:2.145–2.185 μm 6:2.185–2.225 μm 7:2.235–2.285 μm 8:2.295–2.365 μm 9:2.360–2.430 μm	10:8.125–8.475 μm 11:8.475–8.825 μm 12:8.925–9.275 μm 13:10.25–10.95 μm 14:10.95–11.65 μm
Ground resolution	15 m	30 m	90 m
Data rate (Mbits/s)	62	23	4.2
Cross-track pointing (°)	±24	±8.55	±8.55
Cross-track pointing (km)	±318	±116	±116
Swath width (km)	60	60	60
Detector type	Si	PtSi-Si	HgCdTe
Quantization (bits)	8	8	12

[a] The numbers indicate the band number.

Table 4
ASTER band ratios for enhancing mineral features.

Mineral feature	ASTER band combination(s)
Ferric iron	2/1
Ferrous iron	5/3 and 1/2
Ferric oxide	4/3
Gossan	4/2
Carbonate/chlorite/epidote	(7+9)/8
Epidote/Chlorite/Amphibole	(6+9)/(7+8)
Amphibole	(6+9)/8 and 6/8
Dolomite	(6+8)/7
Carbonate	13/14
Sericite/Muscovite/Illite/Smectite	(5+7)/6
Alunite/Kaolinite/Pyrophyllite	(4+6)/5
Phengite	5/6
Kaolinite	7/5
Silica	11/10, 11/12, 13/10
SiO_2	13/12, 12/13
Siliceous rocks	(11 × 11)/(10 × 12)

Source of data: A selection from: http://www.ga.gov.au/image_cache/GA7833.pdf.

Several band ratios have been proposed to map mineral indices (Cudahy and Hewson, 2002):

- Silica index → band 11/band 10, band 11/band 12, band 13/band 10;
- Biotite-epidote–chlorite–amphibole index → (band 6 + band 9)/(band 7 + band 8);
- Skarn carbonates–epidote index → (band 6 + band 9)/(band 7 + band 8), band 13/band 14;
- Garnets-pyroxenes index → band 12/band 13;
- Iron oxide index → band 2/band 1;
- White micas Al-OH depth → (band 5 + band 7)/band 6;
- Carbonates Mg OH depth → (band 6 + band 9)/(band 7 + band 8);
- Carbonate abundance → band13/band14.

A comprehensive overview of mineral indices that can be derived from ASTER data is the 'ASTER Mineral Index Processing Manual' compiled by Aleks Kalinowski and Simon Oliver (http://www.ga.gov.au/image_cache/GA7833.pdf). These authors suggest a range of band combinations and ratios for mapping various mineral assemblages in relation to different styles of alteration (Table 4) and false color composites that highlight alteration intensity (Table 5). In addition, the ASTER team proposed an empirical silica index using the ASTER TIR bands formulated as (Watanabe, 2002):

$$SiO_2(\%) = 56.20 - 271.09 \times \mathrm{Log}((\mathrm{Ems}[10] + \mathrm{Ems}[11] + \mathrm{Ems}[12])/3), \quad (2)$$

where Ems[n] is the emissivity of ASTER band n. A Calcite-, Alunite-, Kaolinite- and Montmorillonite-index based on linear combinations of ASTER SWIR bands was presented and tested on ASTER data from the Cuprite mining area in Nevada (Yamaguchi and Naito, 2003). Analysis of resampled ASTER spectra on magnetite quartzite and associated lithologies of garnet-ferrous pyroxene granulite, hornblende biotite gneiss, amphibolite, dunite, and pegmatite showed absorption features around the ASTER spectral bands 1, 3, 5, and 7. A RGD color composite image of ASTER band ratios ((1+3)/2, (3+5)/4, (5+7)/6) was used to successfully map these sequences (Rajendran et al., 2011).

The ASTER SWIR bands allow to some extent the mapping of surface mineralogy (provided that the data are transformed to surface reflectance and provided that mineral occurrences are relatively large so that they can be 'seen' at the spatial footprint of ASTER). A recent study (Mars and Rowan, 2010), which compares ASTER image spectra to a spectral library for two alteration areas (e.g., Cuprite, Nevada and Mountain Pass, CA, USA), showed that on the basis of spectrum matching results that advanced minerals groups including argillic minerals (kaolinite, alunite, dickite), phyllic alteration minerals (sericite) and propylitic minerals (calcite, epidote, chlorite) can be separated. However, this study also concluded that detailed mapping of kaolinite versus alunite is not possible. Examples of ASTER geologic data products for the Rodalquilar site are shown in Fig. 5.

Table 5
ASTER False color composites for enhancing mineral features.

Mineral feature	Red	Green	Blue
Advanced argillic alteration	5/6 (phengite)	7/6 (Muscovite)	7/5 (Kaolinite)
Gossan, alteration host rock	4/2 (Gossan)	4/5 (Altered)	5/6 (Host rock)
Gossan, alteration host rock	6 (Gossan)	2 (Altered)	1 (Host rock)
Silica, carbonate	(11 × 11)/(10 × 12)	13/14	12/13
Silica	11/10	11/12	13/10
Product for geologic mapping	4/1	3/1	12/14
Mapping sulfidesulfide rich areas	12	5	3
Enhancing structures	7	4	2

Source of data: A selection from: http://www.ga.gov.au/image_cache/GA7833.pdf.

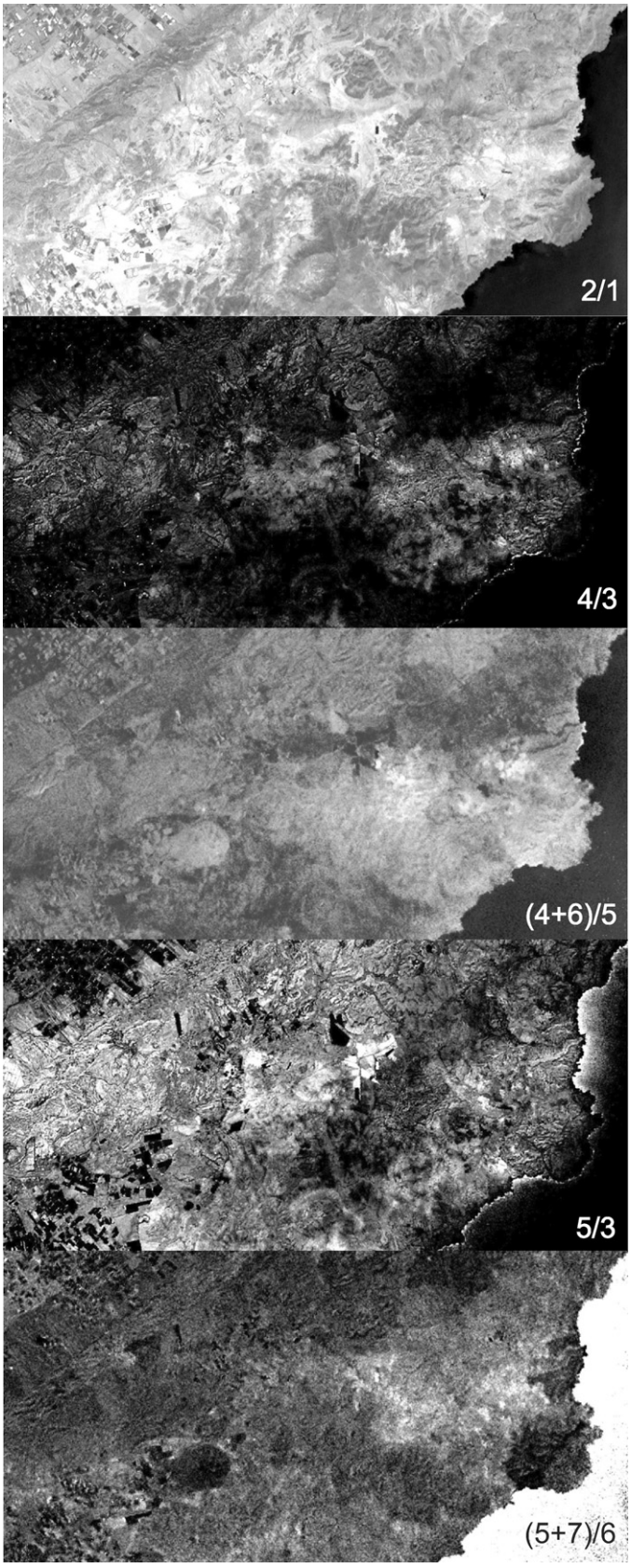

Fig. 5. Examples of ASTER geologic data products for the Rodalquilar site (from top to bottom): 2/1 band ratio, 4/3 band ratio, (4 + 6)/5 band ratio, 5/3 band ratio, (5 + 7)/6 band ratio.

There is a wealth of literature on the use of ASTER data in various geologic settings. Most of these studies are based on single ASTER scenes, but there are also regional geologic mapping projects targeted to mineral prospectivity of mining regions that apply seamlessly merged data sets of over 100 ASTER scenes (Rockwell and Hofstra, 2008; Hewson et al., 2005). ASTER has been extensively used for lithologic mapping (Li et al., 2007; Qiu et al., 2006; Rowan and Mars, 2003; Gomez et al., 2005; Khan et al., 2007). There are several papers on granites (Massironi et al., 2008; Watts et al., 2005), ophiolite sequences (Qiu et al., 2006; Khan et al., 2007) and basement rocks (Qari et al., 2008; Gad and Kusky, 2007; Vaughan et al., 2005). Although ASTER is widely used by the oil and gas industry there are few scientific articles on its applicability. An integrated study using ASTER and several other satellite sensor data sets to map sedimentary terrains in Southern Tunisia illustrates the potential of ASTER data (Pena and Abdelsalam, 2006). Most papers centre on the use of ASTER for mineral exploration with emphasis on geothermal (Vaughan et al., 2005), hydrothermal (Zhang et al., 2007; Hubbard et al., 2003; Yamaguchi and Naito, 2003; Carranza et al., 2008; Mars and Rowan, 2006, 2010), carbonatites (Mars and Rowan, 2011), barite mineralization (Madani and Emam, 2011) and evaporate systems (Kavak, 2005; Oztan and Suzen, 2011). Some works focus on the more generic lithology mapping (Haselwimmer et al., 2011) and ASTER was also used to map granitoids in western Nepal by establishing a relationship between the presence of lichens and these granitoid bodies (Bertoldi et al., 2011).

A new application of ASTER data is related to mapping the mineralogic composition of dune fields (Scheidt et al., 2011). By means of a spatial interpolation of sample compositions, visual interpretation of image data revealed sand transport pathways and gradients of composition between the dune field and surrounding local sources.

An interesting application of ASTER data is found in measuring surface displacements over time by co-registration of optically sensed images and measuring the spatial (de)correlation. This so called COSI-Corr method (Ayoub et al., 2009; Leprince et al., 2007) allows to measure the horizontal displacement vector along faults and provides information similar to radar interferometry. The technique is similar to the subpixel displacement mapping approach using SPOT images discussed earlier.

4. The hyperspectral ERA

4.1. Background

Reflectance spectra of minerals are dominated in the VNIR wavelength range by the presence or absence of transition metal ions (e.g., Fe, Cr, Co, Ni) resulting in absorption features due to electronic processes. The presence or absence of water and hydroxyl, carbonate and sulfate determine absorption features in the SWIR region due to vibrational processes. In addition, absorption band depth is related to grain or particle size, as the amount of light scattered and absorbed by a grain is dependent on grain size. A larger grain has a greater internal path where photons may be absorbed. On the contrary in smaller grains there are proportionally more surface reflections compared to internal photon path lengths, if multiple scattering dominates, the reflectance decreases with increasing grain size. As the grain size becomes larger, more light is absorbed and the reflectance drops. In general, absorption band depth is correlated with the (relative) amount of material present. Based on relative absorption depth, for example, it has been shown that kaolinite content can be derived with an accuracy of about 2% by weight and organic carbon can be quantified with an accuracy of about 2 wt.% (Kruger et al., 1998).

Absorption of energy and thus the presence of absorption features in reflectance spectra due to electronic processes (e.g., $Fe^{2+} \rightarrow Fe^{3+}$ transitions) manifests in the VNIR part of the spectrum in broad and rather shallow features. Vibration gives rise to narrow and more pronounced features in the SWIR (as overtone features of mid infrared and longwave infrared absorption) roughly at 1.400 μm combined with 1.900 μm due to molecular water, 1.400 μm due to OH−, 2.200 μm due to Al-OH, 2.300 μm due to Mg-OH and 2.320–2.350 μm due to Ca CO_3.

The objective of hyperspectral remote sensing (also referred to as imaging spectrometry or imaging spectroscopy) is to measure quantitatively the components of the Earth System from calibrated (radiance, reflectance or emissivity) spectra acquired as images in many, narrow and contiguous spectral bands. For geologic applications this is done by using spectral absorption features to map Earth surface composition (in terms of mineralogy or lithology) or to quantify rock or soil chemistry or physics using derivative image products.

4.2. Sensors

The first scanning imaging spectrometer was the Scanning Imaging Spectroradiometer (SIS) constructed in the early 1970s for NASA's Johnson Space Centre. After that, civilian airborne spectrometer data were collected in 1981 using a one-dimensional profile spectrometer developed by the Geophysical Environmental Research Company which acquired data in 576 channels covering the 0.4–2.5 μm wavelength followed by the Shuttle Multispectral Infrared Radiometer (SMIRR) in 1981. The first imaging device was the Fluorescence Line Imager (FLI) developed by Canada's Department of Fisheries and Oceans in 1981. NASA's Jet Propulsion Laboratory developed the Airborne Imaging Spectrometer (AIS) of which the first version became operational in 1983 (128 spectral bands, 1.2–2.4 μm, 32 pixels across-track for AIS-1 and 64 for AES-2). Since 1987 to date NASA operates the Airborne Visible/Infrared Imaging Spectrometer (Vane et al., 1993), AVIRIS (224 bands, 0.4 to 2.5 μm region, sampling interval and resolution <10 nm, FOV 30°, 614 pixel swath).

Several companies develop hyperspectral sensors. The Finnish Spectral Imaging (SPECIM) manufactures the AISA (Airborne Imaging Spectrometer for Applications) Family of Airborne Imaging Spectrometers (the AisaEAGLE, VNIR 0.400–0.970 μm, 512 or 1024 spatial pixels, 488 spectral bands; AisaHAWK, SWIR 0.970–2.500 μm, 320 spatial pixels, 254 spectral bands; AisaOWL, 8–12 μm, 384 pixels, 84 spectral bands). In Canada, ITRES developed the Compact Airborne Spectrographic Imager (CASI), operational since 1989 (288 spectral channel, 1.9 nm. resolution, 512–1500 pixels across track, 400–1100 range) and similar systems in the SWIR (SASI), MIR (MASI) and TIR (TASI). The Geophysical Environmental Research Corporation (GER) developed the GER Imaging Spectrometer (GERIS), the Digital Airborne Imaging Spectrometer (DAIS; 72 channels, 0.4–2.5 μm, FOV of 3.3 mrad and six channels in the 8–12 μm region). The Australia-based company Integrated Spectronics designed the HYperspectral MAPper (HyMAP; in the U.S. known as Probe-1) a 126 channel sensor covering the 0.4–2.5 μm region.

The first satellite imaging spectrometer was the LEWIS Hyperspectral Imager (HSI) from TRW company which was launched in 1997 but failed. Within the framework of the New Millennium Program NASA launched Hyperion on New Millennium Program (NMP) Earth Observing (EO)-1. Hyperion (Pearlman et al., 2003), being based on the LEWIS concept, has 220 spectral bands (from 0.4 to 2.5 μm) with a 30 m spatial resolution imaging a 7.5 km by 100 km area per frame flying a 705 km circular sun-synchronous orbit at a 98.7° inclination which allows to match within one minute the Landsat 7 orbit. The European Space Agency currently operates the Compact High Resolution Imaging Spectrometer, CHRIS (Barnsley et al., 2004), on board the Proba-1 (9 years of operation) which measures directional spectral reflectance using multiple viewing and illumination geometries, a spectral range of 0.415–1.050 μm, a spectral resolution of 5–12 nm with up to 19 spectral bands and a spatial resolution of 20 m at nadir on a 14 km swath.

At present, GFZ and DLR are developing a hyperspectral spaceborne instrument under the Environmental Mapping and Analysis Programme (ENMAP). ENMAP (Stuffler et al., 2007) will be a dedicated imaging pushbroom hyperspectral sensor covering the spectral range from 0.430 to 0.950 μm (VNIR) and from 0.950 to 2.400 μm (SWIR) with 184 channels, a swath width of 30 km at high spatial resolution of 30 m and off-nadir (30°) pointing feature for fast target revisit (<3 days). The present design concept (Guanter et al., 2009b, Segl et al., 2010) foresees in 89 bands from 423 to 994 nm and 155 bands from 905 to 2446 nm using fast targeting revisit using tilt mode (±30°), thus reaching a 4-day revisit. Tentative launch is scheduled for April 2015.

Another spaceborne hyperspectral sensor under design is the PRISMA mission (700 km orbit, 20–30 m resolution, swath width of 30–60 km, 0.4–2.5 μm continuous coverage with 10 nm bands) to be launched in 2012 by the Italian Space Agency. ESA is preparing under the GMES programme the Sentinel-2 mission which carries a MultiSpectral Imager (MSI) with a swath of 290 km, providing 13 spectral VNIR-SWIR bands (four spectral bands at 10 m, six bands at 20 m and three bands at 60 m spatial resolution). NASA is currently working on the HYpSPectral InfRared Imager (HyspIRI) mission (tentative launch in 2020); an imaging spectrometer that measures from the VNIR to SWIR and a TIR imager both at a spatial resolution of 60 m at nadir. For a review on spaceborne hyperspectral missions consult (Buckingham and Staenz, 2008).

The hyper–multi spectral mission named HISUI (Hyperspectral Imager SUIte), formerly Hyper-X, is a Japanese hyperspectral mission on board the ALOS-3 satellite. HISUI is the follow up mission of ASTER and specifications now foresee in 57 VNIR bands (0.4–0.97 μm at 10 nm resolution) and 128 SWIR bands (0.9–2.5 μm at 12.5 nm resolution) at a 30 m spatial resolution and 30 km swath (Kawashima et al., 2010). Tentative launch is set for 2014.

There are two hyperspectral imagers that are circling the planet Mars that are noteworthy to mention: CRISM and OMEGA. The Compact Reconnaissance Imaging Spectrometer for Mars (CRISM) on the Mars Reconnaissance Orbiter (Murchie et al., 2007) covers the VNIR wavelengths (0.37–3.92 μm) and produces several summary products including those capturing surface mineralogical information (Pelkey et al., 2007). The OMEGA hyperspectral imager (OMEGA stands for Observatoire pour la Mineralogie, l'Eau, les Glaces, et l'Activite) on board ESA's Mars Express mission, is dedicated to surface compositional mapping of Mars at a 0.3–5 km. resolution (Bibring et al., 2005).

4.3. Processing

The pre-processing chain of hyperspectral data includes preflight laboratory calibration and in-flight calibration of the sensor to establish the relationship between photon counts on the detector and (spectral) radiance and to model the spectral response functions for each channel and the point spread function of the sensor. Several authors provide an overview of the pre-processing chain for hyperspectral data (Schaepman et al., 2009; van der Meer et al., 2009) or radiometric calibration principles (Kohler et al., 2004). In most cases, the end user is provided with at-sensor radiance data which then need to be atmospherically corrected and subsequently geocoded. Most airborne systems carry onboard GPS and inertial navigation systems (INS) the first providing geographic coordinates during image acquisition and the latter

providing attitude information on the aircraft together allowing precise geocoding of the data. Removal of atmospheric effects (scattering and absorption as well as terrain illumination effects) is done through absolute correction methods using radiative transfer codes (Guanter et al., 2009a, Richter, 1996; Richter et al., 2002; Richter and Schlapfer, 2002) or empirical correction using scene information only (Ben-Dor and Levin, 2000) and/or field measurements (Ferrier, 1995).

The advent of high spectral resolution sensors led to the development of a new suite of techniques to extract information from spectra with the ultimate goal of deriving surface compositional information on the Earth's surface. There are two broad categories of analytical techniques that were developed and that are used widely for classifying hyperspectral data: spectrum matching techniques and subpixel methods (van der Meer, 2006a).

Spectrum matching techniques aim to express the spectral similarity of reference (library or field spectra of known materials) to test (image) spectra. One of the most used techniques is the spectral angle mapper, SAM (Kruse et al., 1993; Hecker et al., 2008), which treats the two spectra as vectors in an n (channel)-dimensional space and calculates the angle between the vectors as a measure of similarity. At small angles this converges to a conventional Euclidian distance. A matching algorithm based on the (cross) correlation of image and reference spectra is the cross correlogram spectral matching technique (van der Meer and Bakker, 1997). More recently a stochastic measure, called the spectral information divergence was proposed (Chang, 2000). The commonly used spectral feature fitting (SFF) approach, that derives a match between library-endmember spectra and pixel spectra based on absorption feature characteristics, recently was used in combination with user-defined constraints in spectral absorption features to extract target information from hyperspectral images (Xu et al., 2011). Also popular image mining approaches such as support vector machines have been applied to hyperspectral data (Mountrakis et al., 2011).

Subpixel methods comprise techniques to unmix hyperspectral images with the aim of quantifying the relative abundance (in fractions, percent or area) of various materials within a pixel. Typically the first step is to find spectrally unique signatures of pure ground components (endmembers), and the second step is to unmix the mixed pixel spectra as (linear or non-linear) combinations of endmember spectra/materials. Assuming the image interpreter has knowledge of the scene or the area to be investigated, endmembers can be extracted directly from target pixels or from spectral libraries. This has the advantage of being a knowledge-based approach, but the disadvantage that certain endmembers may be overlooked which gives errors in the statistical deconvolution of the image. Alternatively there are statistical techniques for endmember selection by which means endmembers can be set to minimize the error of unmixing a scene based on the overall scene variance (Tompkins et al., 1997; van der Meer, 1999) or by comparing spectral mixtures from library spectra to mixed pixel signals (Dennison and Roberts, 2003). An endmember search technique that incorporates spectral scene information in combination with spatial image structure was recently proposed (Zortea and Plaza, 2009). A popular technique has been the pixel purity index (PPI). PPI derives a statistic for each pixel in a hyperspectral scene based on its proximity to a vertex in an n-dimensional feature space assuming that pixels that are closer to these vertices are more likely to represent pure materials. Recently an outline of a fast pixel purity index was given (Chang and Plaza, 2006), and a review paper on PPI was published (Martinez et al., 2006). Some of the early algorithms on spectral unmixing (Settle and Drake, 1993; Shimabukuro and Smith, 1991; Harsanyi and Chang, 1994) assumed linearity among endmembers and used least squares regression analysis for estimating fractions. Coming from the field of fuzzy classification, Foody was among the first to acknowledge the problem of non-linearity and introducing non-linear unmixing (Foody et al., 1997) which too date has found its way into many algorithms and paper (Nielsen, 2001; Plaza et al., 2004).

Table 6
Summary of the main spectrally active minerals in relation to different alteration styles and environments of formation.

Environment of formation	Main spectrally active alteration minerals
High sulfidation epithermal	Alunite, pyrophyllite, dickite, kaolinite, diaspore, zunyite, smectite, illite
Low sulfidation epithermal	Sericite, illite, smectite, chlorite, carbonate
Porphyry: Cu, Cu-Au	Biotite, anhydrite, chlorite, sericite, pyrophyllite, zeolite, smectite, carbonate, tourmaline
Carlin-type	Illite, dickite, kaolinite
Volcanogenic massive sulfide	Sericite, chlorite, chloritoid, carbonates, anhydrite, gypsum, amphibole
Archean Lode Gold	Carbonate, talc, tremolite, muscovite, paragonite
Calcic skarn	Garnet, clinopyroxene, wollastonite, actinolite
Retrograde skarn	Calcite, chlorite, hematite, illite
Magnesium skarn	Fosterite, serpentine-talc, magnetite, calcite

4.4. Applications in geology: the VIS-SWIR range

The driver for applications of hyperspectral remote sensing in geology has been and still are is mineral mapping and the retrieval of surface compositional information for mineral exploration purposes. Often this is related to hydrothermal systems (Huntington, 1996). Fig. 6 (Sillitoe, 1996, 2010) gives a schematic overview of intrusion related alteration systems and associated mineral deposits. Table 6 gives an overview of spectrally active and most abundant minerals for different alteration settings and related mineralizations. These can be translated through combinations of key absorption features into areas in the VIS-SWIR spectrum where diagnostic information is found for mapping these mineral assemblages (Fig. 7).

The most frequently studied systems are hydrothermal as these include abundant spectrally active mineral groups such as hydroxyl-bearing minerals (hydrothermal clays, sulfates), ammonium-bearing minerals, phyllosilicates, iron oxides, and carbonates. A classic and well studied hydrothermal system is the NASA-JPL test site at the Cuprite mining district of Nevada where some early work (Abrams et al., 1977) on spectroscopy laid the foundation for the definition of the Landsat, ASTER and subsequently hyperspectral sensors. The literature on hyperspectral remote sensing is dominated by the study of (low and high sulfidation) epithermal gold systems (Crosta et al., 1998; Kruse et al., 2006; Chen et al., 2007; Rowan et al., 2000; Gersman et al., 2008; Bedini et al., 2009; van der Meer, 2006b) most of which use techniques for alteration mineral to study the mineral prospectivity of fossilized systems. A cascaded approach using ASTER data for regional alteration mapping and local follow-up by Hyperion for target selection was presented as a tool for mineral exploration (Bishop et al., 2011). More recently, active hydrothermal systems have been investigating in the context of geothermal energy resources (Vaughan et al., 2005; Yang et al., 2000, 2001; Kratt et al., 2010; Hellman and Ramsey, 2004). Fig. 8 shows mineral maps for key alteration minerals in Rodalquilar.

There are fewer studies on other deposit types although most common deposit types have been characterized and analyzed with hyperspectral data including: Carlin-type systems based on

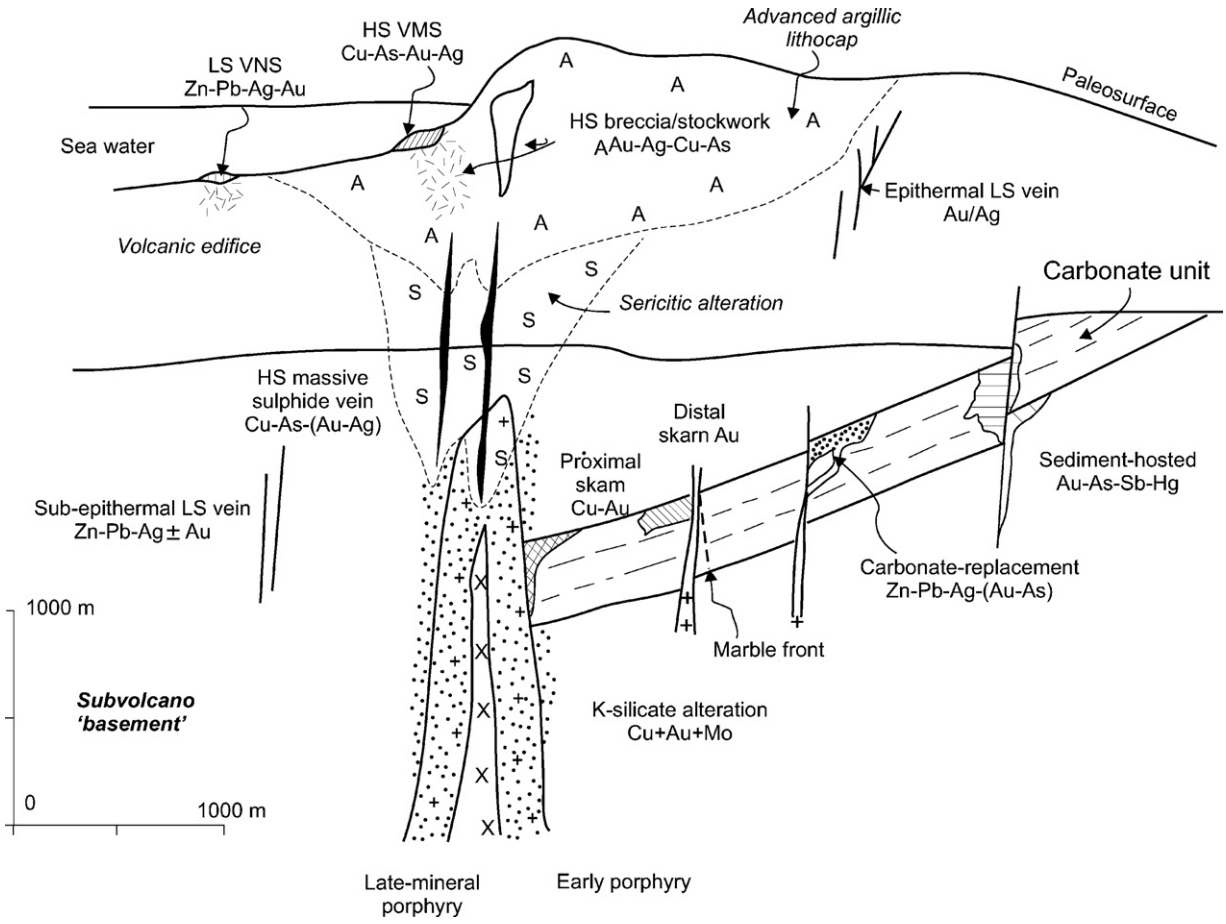

Fig. 6. The occurrence of mineral deposits and alteration styles related to submarine volcanism in granite related setting and porphyry copper systems. *Source*: Sillitoe (1996); Sillitoe (2010); Modified after unpublished data from Anne Thompson and personal communication of Phoebe Hauff.

hyperspectral field measurements using ASTER (Rockwell and Hofstra, 2008), Archean lode (Bierwirth et al., 2002), skarns (Windeler, 1993), Calcic skarn (Kozak et al., 2004; Rowan and Mars, 2003; Bedini, 2009), and volcanogenic massive sulfide ore (VMS) deposits (Berger et al., 2003). The emphasis of these papers is on mapping surface mineralogy and using these mineral as vectors to ore. An interesting application is the use of spectroscopy to aid in sulfidesulfide ore grading in VMS deposits (Gallie et al., 2002). Although some of the early studies on absorption feature position in relation to Tschermak substitution (Duke, 1994) showed that chemical composition of micas and chlorites can be related to subtle wavelength shifts related to compositional changes in Na versus K and Al versus Mg. Very little has been done with this in terms of mapping. Recently (Duke and Lewis, 2010) this work progressed in the direction of assessing the metamorphic grade of rocks but mapping of these subtle spectral shifts has not been demonstrated. There are some papers that link spectroscopy to mineral chemistry to reconstruct fluid pathways (van Ruitenbeek et al., 2005, 2006), several researchers have used the carbonate absorption feature to map calcite- dolomite mineralogy (Gaffey, 1986; van der Meer, 1996) and dolomitization patterns (Windeler and Lyon, 1991). Earth analogues of hydrothermal systems have been demonstrated to be proxies for understanding the surface mineralogy of the planet Mars. Several researchers have suggested that hydrothermal systems exist on Mars, but, that these are formed under much lower average surface temperatures than comparable geological settings on Earth (Farmer, 1996). More recent studies revealed the presence of sulfates (Wang et al., 2006; Mangold et al., 2008; Aubrey et al., 2006), hydrated silicates (Mustard et al., 2008; Ehlmann et al., 2009) and phyllosilicates (Loizeau et al., 2007) on Mars supporting

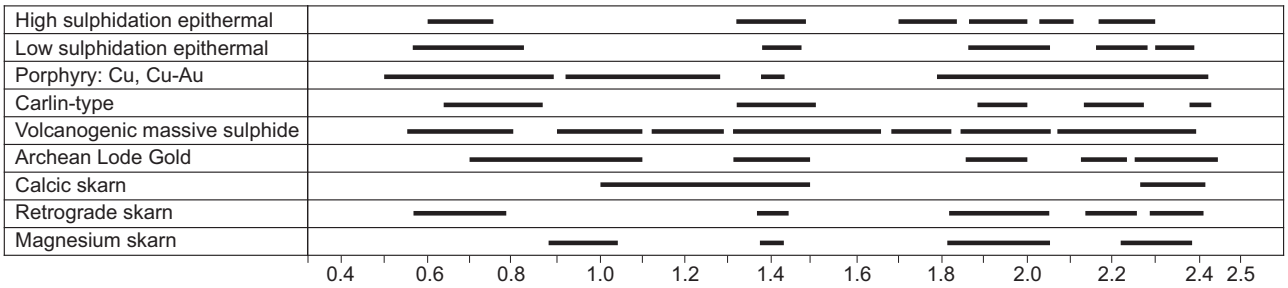

Fig. 7. Summary of the main deposit types in relation to areas in the spectrum (indicated by the bars) where absorption occurs related to the presence of key alteration minerals.

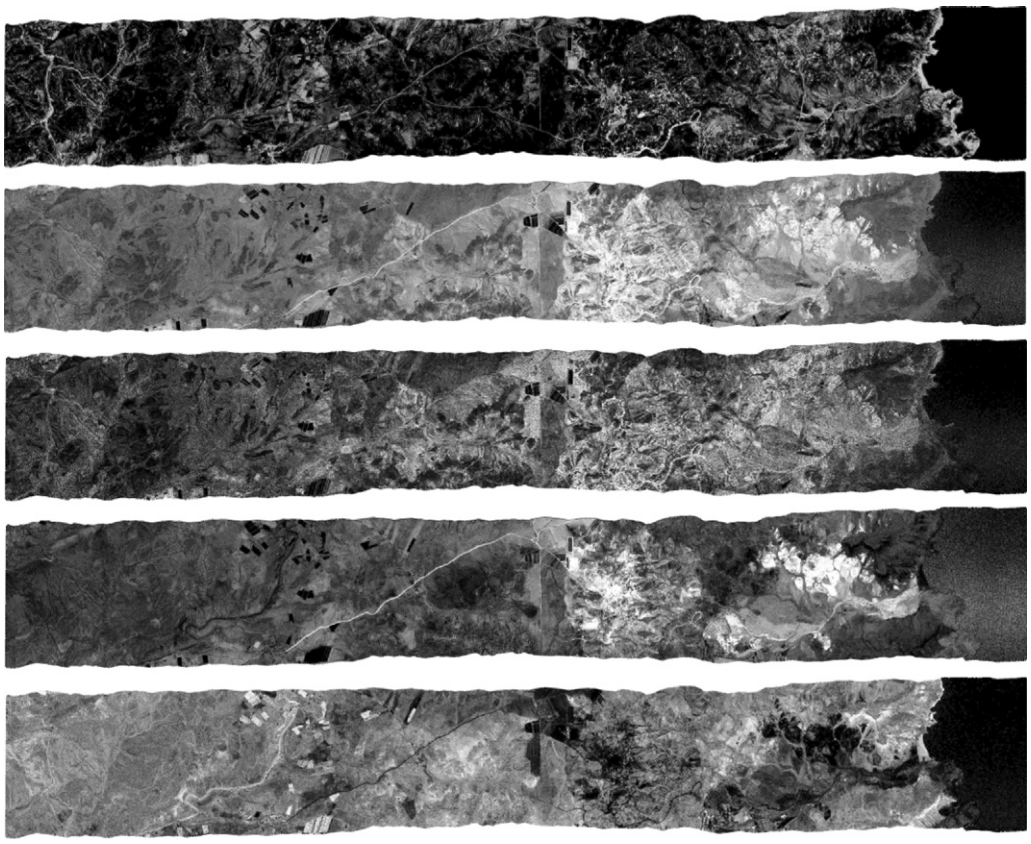

Fig. 8. Mineral maps for key alteration minerals in Rodalquilar mapped using HyMAP (from top to bottom): jarosite, kaolinite, illite, alunite, chlorite.

the idea of hydrothermal processes on Mars although sulfates could also be evaporitic in nature.

There are some studies on the use of hyperspectral remote sensing for lithologic mapping in Arctic conditions (Harris et al., 2005), in a granitic terrain (Rivard et al., 2009), in an ophiolite sequence (Roy et al., 2009) and in peridotites (the Ronda peridotite, SE Spain) (Chabrillat et al., 2000; Launeau et al., 2004).

Hyperspectral remote sensing is also frequently used to study mine tailings (Choe et al., 2008; Shang et al., 2009; Riaza and Muller, 2010; Richter et al., 2008; Mars and Crowley, 2003). Most studies focus on acid-generating minerals in tailings such as pyrite and map the spatial distribution of the oxidation product (e.g., jarosite, ferrihydrite, goethite/hematite) as an indicator of environmental pollution level. These studies focus primarily on mapping of surface mineralogy and largely neglect aspects of environmental quality, aspects of health and the link of surface leaching to element mobility and transportation in groundwater. There are few studies that combine hyperspectral maps with aspects of health with the exception of a study that mapped asbestos minerals occurring in dust form that could be blown by wind and form a threat to human health (Swayze et al., 2009).

There are few attempts to link hyperspectral remote sensing to the oil & gas industry. Most of these relate to studying (detection and characterization through surface mineral mapping) oil seeps (Horig et al., 2001; Kuhn et al., 2004) and gas seeps (van der Meer et al., 2002; van der Werff et al., 2006) and to mapping oil sands and estimating the total bitumen content of these sands (Lyder et al., 2010).

Most of the above studies use airborne hyperspectral data sets where AVIRIS and HyMAP are the most frequently used instruments. Kruse (Kruse et al., 2003) used Hyperion spaceborne hyperspectral data and compared it to AVIRIS data and concluded that "spaceborne hyperspectral sensors can produce useful mineralogic information, but also indicate that signal-to-noise ratio (SNR) improvements are required for future spaceborne sensors to allow the same level of mapping that is currently possible from airborne sensors such as AVIRIS". Some research supports this statement including work on the comparison of the use of Advanced Land Imager (ALI), ASTER, and Hyperion data for mineral mapping (Hubbard et al., 2003) and work on the use of Hyperion data for mapping hydrothermal alteration (Gersman et al., 2008). Recently, Hyperion was used to produce stratigraphic classification products through a processing chain that included smile correction resulting in an updated geologic map for the Dana Geology National Park in Jordan (Dadon et al., 2011).

An interesting development of hyperspectral technology is drill core imaging and wall rock imaging. The first published study on hyperspectral drill core analysis dates back to 1996 and used the PIMA spectrometer (Kruse, 1996). Presently there are several drill core imaging facilities that provide scanned hyperspectral data on drill core. Although these become more and more readily used by the mining industry to determine metal grades and separate ore from waste, there are few scientific publications on this technique (Gallie et al., 2002; Bolin and Moon, 2003; Brown et al., 2008). A logical extension to this is terrestrial hyperspectral sensing which allows to image wall rock and outcrops. Again this is an application of hyperspectral remote sensing that is very promising as it (1) fills a gap between field point-based measurements and image data and (2) it allows to measure vertical faces that are not easily imaged from an airborne platform, however on which few publications exist (Ragona et al., 2006).

Although this review concentrates on geologic remote sensing applications on Earth it is noteworthy to mention that hyperspectral observations have led to scientific breakthroughs in mapping

and understanding surface composition in planetary geology. In recent years, several studies using CRISM and OMEGA data have shed new light on the geology of Mars. Occurrences of phyllosilicates indicate that hydrothermal processes and/or weathering have acted on the Martian surface. Several types of phyllosilicate minerals have been positively identified on Mars using VNIR imaging spectroscopy (Bibring et al., 2005; Poulet et al., 2005). Fe, Mg and Al-smectites (nontronite, saponite, and montmorillonite) are most abundant, minor occurrences of kaolinite, rich chlorites (Fe-rich chamosite and Mg chlorites) and illite/muscovites have also been reported. Presence of phyllosilicates is generally restricted to rocks of Noachian age though some have been detected in rocks of early Hesperian age. Phyllosilicate deposits have mainly been found in three different forms: (1) As layered phyllosilicate deposits, (2) as massive Noachian phyllosilicate deposits, and (3) phyllosilicate-containing intracrater fans. Genetic mechanisms for the formation of these deposits are unknown though several have been proposed including alteration of volcanic ash, subaerial weathering of basaltic regolith, subaqueous sedimentation of sorted transported clays (Loizeau et al., 2007) and hydrothermal deposition. In addition, also sulfates (Gendrin et al., 2005) and olivine/pyroxene (Mustard et al., 2005) have been mapped.

4.5. Applications in geology: the TIR range

Emissivity spectroscopy provides information that is synergistic to spectroscopy in the VNIR-SWIR as several key rock/soil forming minerals (quartz, feldspars, olivines and pyroxenes) that are spectrally featureless in the VNIR-SWIR have diagnostic absorption features in the TIR range. The TIR (8–14 μm) and the MIR (3–5 μm) are areas that have great potential for geologic remote sensing studies, but that have been under-investigated probably due to (1) the complexity of the physics (e.g., volume scattering effects in the TIR and emissivity and temperature interference in the MIR) and (2) lack of field/laboratory spectrometers and (airborne/spaceborne) hyperspectral data. In the early 1990s, Mike Abrams showed the added value of combined TIR and SWIR observations (Abrams et al., 1991; Hook et al., 1998). From TIR multispectral scanner data Simon Hook and co-authors showed the type of information that could be revealed (Hook et al., 1992, 1994; Hook and Kahle, 1996). The work on TIR spectroscopy of minerals and rocks (Salisbury and Daria, 1992; Salisbury and Walter, 1989; Salisbury et al., 1989) and mid infrared spectroscopy (Salisbury and Daria, 1994) of John Salisbury and his group has been instrumental to the development field of thermal remote sensing. His fundamental work showed the potential of this region particularly in emissivity measurements and also the complexity of physics. Much of this work has been collected in the standard library (4000 copies, ~2000 spectra) for emissivity spectra: the ASTER spectral library (Baldridge et al., 2009). Recently, a review of TIR emissivity spectra of feldspars was published (Hecker et al., 2010) emphasizing that feldspars are economically important as industrial minerals and as a vector-to-ore for mineral deposits.

There are several satellite missions that currently acquire image data in the TIR region at varying spatial and temporal resolutions including ASTER (90 m, 16-day repeat), MODIS (the Moderate Resolution Imaging Spectroradiometer, 1 km, daily revisit), SEVIRI/MSG (the Spinning Enhanced Visible and Infrared Imager, 3 km, 15 min), AVHRR-3/METOP (the Advanced Very High Resolution Radiometer, 1.1 km, daily revisit). Although these allow deriving land surface temperature, the spatial and spectral resolutions are too coarse to accurately measure emissivity. In addition, there are a number of missions planned such as NASA's HyspIRI mission (60 m, 1-week revisit), SLSTR on ESA's SENTINEL-3 mission (the Sea and Land Surface Temperature Radiometer, 500–1 km resolution) and there are several airborne instruments that can be deployed including the AHS (the airborne hyperspectral scanner), ITRES Sasi-600, Specim AISA Owl, and SEBASS (the Spatially Enhanced Broadband Array Spectrograph System).

Use of TIR data for geologic mapping has focused on data from SEBASS (Vaughan et al., 2003, 2005; Kirkland et al., 2002). In addition, there are several studies on TIR mineral mapping on Mars using the Thermal Emission Spectrometer (TES) on the Mars Global Surveyor mission (Christensen et al., 2001; Bandfield, 2002).

5. Discussion and conclusions

In a personalized view on the development of the field of hyperspectral remote sensing one of the founders of geologic remote sensing, Alexander Goetz (Goetz, 2009), recognized four trends (and needs) which can be summarized as (1) a need for more accurate measurements where (airborne) hyperspectral data adds to high spectral resolution coarse footprint sensors like MODIS and MERIS, (2) a need for education in remote sensing and hyperspectral RS to create awareness of the technique, (3) to need to explore the advance of sensor technology and computing power to advance sensor capabilities and (4) a need for a hyperspectral instrument in orbit. Adding to this a number of issues can be raised.

5.1. Validation issues

The past decades have shown a trend toward higher spectral resolution (hyperspectral remote sensing) and toward band positioning on key absorption features (ASTER). Hyperspectral remote sensing is defined as 'acquiring images in many, narrow and contiguous spectral bands to reconstruct a full spectrum that can be compared directly to field or laboratory spectra'. Herein lies both the strength as well as the weakness of the technique. The strength of the availability of hundreds of spectral bands is that it (1) allows mimicking reflectance or radiance spectra acquired in the field, (2) allows cross comparison to field data, and (3) allows catering for many different applications. However the weaknesses are (1) the engineering challenge to acquire such data at sufficient quality (in terms of SNR, NER), which has been a problem for spaceborne acquisition, (2) the complexity of the calibration and pre- and post-processing of the data, (3) the data redundancy due to channel overlap of adjacent channels in each sensor, and (4) the data redundancy due to acquisition in spectral regions that are of little user interest. The lack of quantitative end products for the geologic community from multispectral and hyperspectral data hampers the use of such data. As opposed to the meteorological sector which uses a model-based approach whereby through data assimilation parameters are estimated based on principles of physics, the geologic remote sensing community primarily uses empirical approaches and estimates parameters through correlation. This hampers the validation and reproducibility of these parameters and makes the results very site specific implying that there is no single recipe that is universally applicable. An attempt to develop automatic procedures leading toward reproducible approaches is the USGS tetracorder (Clark et al., 2003) expert system rules that describe which diagnostic spectral features are used in the decision making process. However the statement 'no single analytical technique can be used to fully deconvolve hyperspectral data in the absence of ancillary data (Cloutis, 1996)' is still true and this hampers automating processing chains and standardized (qualitative or quantitative) products.

5.2. Bridging the gap between Earth observation science and Earth science

The geologic remote sensing community has a bias to publishing results in remote sensing journals. If the papers referenced

in this Article are a representative set of the entire population of science output in this field then 40% is published in geosciences journals (26% Earth science and 14% geophysics journals) and 60% is published in remote sensing journals with *International Journal of Remote Sensing* and *Remote sensing of Environment* having a 'market-share' of, 20% and 16%, respectively, of the total. More importantly, whereas in adjacent fields (e.g., biology and hydrology), there is a trend toward retrieval of chemical and physical land surface parameters (i.e., from NVDI to FPAR and biochemicals), the geologic remote sensing community persistently has focused on lithology, alteration and surface mineralogy. There is a strong and direct link between reflected radiation and mineralogy through quantum physical processes that have been duly explored by the community. However, it is our firm belief that bridging the gap between Earth observation science and Earth science and increasing the visibility and usefulness of geologic remote sensing products we should put more emphasis on retrieving chemical (element, whole rock geochemistry) and physical (temperature and pressure in relation to metamorphic processes) variables to complement the lithologic, mineralogic and structural information. On the contrary, geologic remote sensing products from both multispectral as well as hyperspectral imaging have found their way to the mining industry and to a lesser extent the oil and gas industry.

5.3. Multidisciplinary approaches

Numerous papers deal with the characterization of mineral deposits and hydrothermal systems by mapping surface alteration mineralogy. This is an important task, but it is not always evident what the added value and new scientific insights are. Very few studies in geologic remote sensing are truly multidisciplinary or interdisciplinary, although by cross-linking with other disciplines new insights are often created. Cross-links that would deserve more attention and may pay off as being scientifically very fruitful are combining geology and health, linking pollution studies to environmental quality, linking spectral surface mineral maps to runoff and erosion models and further exploiting the relation between geology and biology. An obvious limitation of remote sensing is that it allows only to characterize the Earth' surface whereas geologic structures are three-dimensional; subsurface information is essential. Coupling surface information from remote sensing imagery with subsurface information from geophysical data has been underexploited by the geologic remote sensing community. Let alone the integration of this three-dimensional information into groundwater models and pollution models for monitoring dispersion. The GIS community and the land use mapping communities using remote sensing data have embarked into object-based image analysis using not only spectral but also spatial or contextual information in images for mapping purposes. Although there is a wealth of papers in this realm (Blaschke, 2010) and a community that is rapidly maturing this technology is not picked up at large in the geologic remote sensing community. In general, monitoring capabilities, which are the added value of Earth observation technology, are seldom used in geologic remote sensing which predominantly uses single observations in time of (airborne) campaign data, thus, neglecting the time-domain which would allow studying processes instead of making inventories.

5.4. Data continuity

The past decade in the field of geologic remote sensing can be characterized by a gradual change of focus from the "inventory" type of science (mapping, databases, what is where?) to the understanding of processes that play a role in shaping our environment, predicting their effects in future and providing improved information support for planning and policy making. Over the past decades we have also seen a closing of the gap between the realms of Earth Observation (satellite observation of the Earth) providing the monitoring capability and the GIS and modeling worlds providing geospatial solutions. Thematically over the past decade the focus on system Earth has shifted from monitoring and forecasting change to adaptation to change which brings the human component and perception into the picture. Alongside, the governance of space has accelerated over the past years and Earth monitoring is now conducted in a structured framework of international policies and governmental initiatives such as the Global Monitoring for Environment and Security (GMES) programme of the European Commission and the European Space Agency (ESA), and the Global Earth Observation System of Systems (GEOSS) initiative. GEOSS priorities are laid down in so-called societal benefit areas including disasters, health, energy, climate, water, weather, ecosystems, agriculture and biodiversity. Through the themes of disaster and energy, geologic remote sensing is more visible than ever.

Effective use of geologic remote sensing products relies on data continuity. In the meteorological and oceanographic sectors this is secured. However data continuity is not a luxury that we can rely on. For decades with the Landsat programme there has been continuity and one can even argue that ASTER was a logical continuity from Landsat ETM+. However with the ASTER SWIR module now failed, and ASTER outlived its planned lifetime by 5 years, it becomes apparent that there will be a gap in observations for the coming years that may eventually be filled by HySPIRI although with a 2020 launch date this is not possible or with the Landsat continuity mission that NASA is planning. Thus likely the superspectral instruments such as the Landsat LDCM or the Sentinel-2 mission should be used by the geologic remote sensing community to ensure data continuity. Alexander Goetz (Goetz, 2009) argues for a hyperspectral imager in orbit that can produce data at the quality and resolution of AVIRIS. Hyperion has been operational since the year 2000. However it is evident that the quality of the data and the complexity of the pre-processing hamper wide usage of this spaceborne hyperspectral resource. ENMAP may in future fulfill this role; however, besides passing on numerous channels to the science community it would also be advantageous to have dedicated products for specific user communities where the geologic user community could request validated surface mineral maps. Thus, for SWIR hyperspectral observations from space there is a future perspective, for TIR hyperspectral remote sensing from space, regardless the added value that emissivity would bring there is no instrument foreseen. Hyperspectral remote sensing has too much the image of being an *ad hoc* campaign-type of technique; it needs to develop a global perspective through global coverage and dedicated products.

Acknowledgements

We have collected a large set of scientific papers where, for the sake of accessibility for the reader, we have largely restricted ourselves to the ISI journal papers. Inevitably we had to make a selection and hence some papers have been omitted as this is the nature of any review. We apologize to those authors whose papers have not been included. This paper resulted from a number of key note presentations that we have given at various conferences including: the Geological Remote Sensing Group (London, UK, 2001), the International Geological Congress (Italy, Florence, 2004), the Geomonitoring in the Energy and Mineral Resources Industry Using Remote Sensing (Freiberg, Germany, 2006), the Brazilian Remote Sensing Congress (Brazil, Natal, 2009), the ESA oil & gas workshop (Italy, Frascati, 2010), and the EARSeL Imaging Spectroscopy workshop (UK, Edinburgh, 2011). Discussions with various researchers in geologic remote sensing helped in shaping the discussion and conclusion section. Without their knowing they

contributed to our thinking. Thanks are due to Mike Abrams (NASA JPL), Tom Cudahy (CSIRO), Andreas Mueller (DLR) and Stuart Marsh (BGS). We gratefully acknowledge the review of the anonymous referees.

References

Abdelsalam, M.G., Stern, R.J., Berhane, W.G., 2000. Mapping gossans in arid regions with landsat TM and SIR-C images: the Beddaho Alteration Zone in northern Eritrea. Journal of African Earth Sciences 30, 903–916.

Abrams, M., 2000. The Advanced Spaceborne Thermal Emission and Reflection Radiometer (ASTER): data products for the high spatial resolution imager on NASA's Terra platform. International Journal of Remote Sensing 21, 847–859.

Abrams, M., Hook, S.J., 1995. Simulated ASTER data for geologic studies. IEEE Transactions on Geoscience and Remote Sensing 33, 692–699.

Abrams, M., Ashley, R., Rowan, L.C., Goetz, A.F.H., Kahle, A.B., 1977. Mapping of hydrothermal alteration in the Cuprite mining district, Nevada, using aircraft scanner imagery from 0.46–2.36 μ spectral region. Geology 5, 713–718.

Abrams, M., Brown, D., Lepley, L., Sadowski, R., 1983. Remote sensing of porphyry copper deposits in Southern Arizona. Economic Geology 78, 591–604.

Abrams, M., Abbott, E., Kahle, A., 1991. Combined use of visible, reflected infrared, and thermal infrared images for mapping Hawaiian lava flows. Journal of Geophysical Research—Solid Earth and Planets 96, 475–484.

Arribas, A., Cunningham, C.G., Rytuba, J.J., Rye, R.O., Kelly, W.C., Podwysocki, M.H., Mckee, E.H., Tosdal, R.M., 1995. Geology, geochronology, fluid inclusions, and isotope geochemistry of the rodalquilar gold alunite deposit, Spain. Economic Geology and the Bulletin of the Society of Economic Geologists 90, 795–822.

Aubrey, A., Cleaves, H.J., Chalmers, J.H., Skelley, A.M., Mathies, R.A., Grunthaner, F.J., Ehrenfreund, P., Bada, J.L., 2006. Sulfate minerals and organic compounds on Mars. Geology 34, 357–360.

Aydal, D., Ardal, E., Dumanlilar, O., 2007. Application of the Crosta technique for alteration mapping of granitoidic rocks using ETM+ data: case study from eastern Tauride belt (SE Turkey). International Journal of Remote Sensing 28, 3895–3913.

Ayoub, F., Leprince, S., Avouac, J.P., 2009. Co-registration and correlation of aerial photographs for ground deformation measurements. ISPRS Journal of Photogrammetry and Remote Sensing 64, 551–560.

Baldridge, A.M., Hook, S.J., Grove, C.I., Rivera, G., 2009. The ASTER spectral library version 2.0. Remote Sensing of Environment 113, 711–715.

Bandfield, J.L., 2002. Global mineral distributions on Mars. Journal of Geophysical Research—Planets, 107.

Barnsley, M.J., Settle, J.J., Cutter, M.A., Lobb, D.R., Teston, F., 2004. The PROBA/CHRIS mission: a low-cost smallsat for hyperspectral multiangle observations of the earth surface and atmosphere. IEEE Transactions on Geoscience and Remote Sensing 42, 1512–1520.

Bedini, E., 2009. Mapping lithology of the Sarfartoq carbonatite complex, southern West Greenland, using HyMap imaging spectrometer data. Remote Sensing of Environment 113, 1208–1219.

Bedini, E., van der Meer, F., van Ruitenbeek, F., 2009. Use of HyMap imaging spectrometer data to map mineralogy in the Rodalquilar caldera, southeast Spain. International Journal of Remote Sensing 30, 327–348.

Ben-Dor, E., Levin, N., 2000. Determination of surface reflectance from raw hyperspectral data without simultaneous ground data measurements: a case study of the GER 63-channel sensor data acquired over Naan, Israel. International Journal of Remote Sensing 21, 2053–2074.

Berger, B.R., King, T.V.V., Morath, L.C., Phillips, J.D., 2003. Utility of high-altitude infrared spectral data in mineral exploration: application to northern Patagonia mountains, Arizona. Economic Geology and the Bulletin of the Society of Economic Geologists 98, 1003–1018.

Bertoldi, L., Massironi, M., Visona, D., Carosi, R., Montomoli, C., Gubert, F., Naletto, G., Pelizzo, M.G., 2011. Mapping the Buraburi granite in the Himalaya of Western Nepal: remote sensing analysis in a collisional belt with vegetation cover and extreme variation of topography. Remote Sensing of Environment 115, 1129–1144.

Bhan, S.K., Bhattacharya, A., Guha, P.K., Ravindran, K.V., 1991. IRS-1A applications in geology and mineral-resources. Current Science 61, 247–251.

Bibring, J.P., Langevin, Y., Gendrin, A., Gondet, B., Poulet, F., Berthe, M., Soufflot, A., Arvidson, R., Mangold, N., Mustard, J., Drossart, P., Team, O., 2005. Mars surface diversity as revealed by the OMEGA/Mars Express observations. Science 307, 1576–1581.

Bierwirth, P., Huston, D., Blewett, R., 2002. Hyperspectral mapping of mineral assemblages associated with gold mineralization in the Central Pilbara, Western Australia. Economic Geology and the Bulletin of the Society of Economic Geologists 97, 819–826.

Bilotti, F., Shaw, J.H., Brennan, P.A., 2000. Quantitative structural analysis with stereoscopic remote sensing imagery. AAPG Bulletin 84, 727–740.

Bishop, C.A., Liu, J.G., Mason, P.J., 2011. Hyperspectral remote sensing for mineral exploration in Pulang, Yunnan Province, China. International Journal of Remote Sensing 32, 2409–2426.

Blaschke, T., 2010. Object based image analysis for remote sensing. ISPRS Journal of Photogrammetry and Remote Sensing 65, 2–16.

Boccaletti, M., Bonini, M., Mazzuoli, R., Abebe, B., Piccardi, L., Tortorici, L., 1998. Quaternary oblique extensional tectonics in the Ethiopian Rift (Horn of Africa). Tectonophysics 287, 97–116.

Bolin, B.J., Moon, T.S., 2003. Sulfide detection in drill core from the Stillwater Complex using visible/near-infrared imaging spectroscopy. Geophysics 68, 1561–1568.

Brown, A.J., Sutter, B., Dunagan, S., 2008. The MARTE VNIR Imaging Spectrometer experiment: design and analysis. Astrobiology 8, 1001–1011.

Buckingham, R., Staenz, K., 2008. Review of current and planned civilian space hyperspectral sensors for EO. Canadian Journal of Remote Sensing 34, S187–S197.

Carranza, E.J.M., van Ruitenbeek, F.J.A., Hecker, C., van der Meijde, M., van der Meer, F.D., 2008. Knowledge-guided data-driven evidential belief modeling of mineral prospectivity in Cabo de Gata, SE Spain. International Journal of Applied Earth Observation and Geoinformation 10, 374–387.

Chabrillat, S., Pinet, P.C., Ceuleneer, G., Johnson, P.E., Mustard, J.F., 2000. Ronda peridotite massif: methodology for its geological mapping and lithological discrimination from airborne hyperspectral data. International Journal of Remote Sensing 21, 2363–2388.

Chang, C.I., 2000. An information—theoretic approach to spectral variability, similarity, and discrimination for hyperspectral image analysis. IEEE Transactions on Information Theory 46, 1927–1932.

Chang, C.I., Plaza, A., 2006. A fast iterative algorithm for implementation of pixel purity index. IEEE Geoscience and Remote Sensing Letters 3, 63–67.

Chavez, P.S., Kwarteng, A.Y., 1989. Extracting spectral contrast in Landsat Thematic Mapper image data using selective principal component analysis. Photogrammetric Engineering and Remote Sensing 55, 339–348.

Chavez, P.S., Berlin, G.L., Sowers, L.B., 1980. Statistical methods for selecting of Landsat MSS ratios. Journal of Applied Photographic Engineering, 8.

Chavez, P.S., Sides, S.C., Anderson, J.A., 1991. Comparison of 3 different methods to merge multiresolution and multispectral data—Landsat TM and SPOT panchromatic. Photogrammetric Engineering and Remote Sensing 57, 295–303.

Chen, X., Warner, T.A., Campagna, D.J., 2007. Integrating visible, near-infrared and short wave infrared hyperspectral and multispectral thermal imagery for geologic mapping: simulated data. International Journal of Remote Sensing 28, 2415–2430.

Choe, E., van der Meer, F., van Ruitenbeek, F., van der Werff, H., de Smeth, B., Kim, Y.W., 2008. Mapping of heavy metal pollution in stream sediments using combined geochemistry, field spectroscopy, and hyperspectral remote sensing: a case study of the Rodalquilar mining area, SE Spain. Remote Sensing of Environment 112, 3222–3233.

Christensen, P.R., Morris, R.V., Lane, M.D., Bandfield, J.L., Malin, M.C., 2001. Global mapping of Martian hematite mineral deposits: remnants of water-driven processes on early Mars. Journal of Geophysical Research-Planets 106, 23873–23885.

Clark, R.N., Swayze, G.A., Livo, K.E., Kokaly, R.F., Sutley, S.J., Dalton, J.B., Mcdougal, R.R., Gent, C.A., 2003. Imaging spectroscopy: Earth and planetary remote sensing with the USGS Tetracorder and expert systems. Journal of Geophysical Research-Planets, 108.

Cloutis, E.A., 1996. Hyperspectral geological remote sensing: evaluation of analytical techniques. International Journal of Remote Sensing 17, 2215–2242.

Cooper, B.L., Salisbury, J.W., Killen, R.M., Potter, A.E., 2002. Midinfrared spectral features of rocks and their powders. Journal of Geophysical Research—Planets, 107.

Crippen, R.E., Blom, R.G., 2001. Unveiling the lithology of vegetated terrains in remotely sensed imagery. Photogrammetric Engineering and Remote Sensing 67, 935–943.

Crippen, R.E., Blom, R.G., Ieee, 1991. Measurement of Subresolution Terrain Displacements using SPOT Panchromatic Imagery. IEEE, New York.

Crippen, R.E., Blom, R.G., Environm Res Inst, M.,1996. Detection, measurement, visualization, and analysis of seismic crustal deformation. In: Proceedings of the Eleventh Thematic Conference: Geologic Remote Sensing—Practical Solutions for Real World Problems, Vol I. Environmental Research Inst. Michigan, Ann Arbor.

Crosta, A.P., McMoore, J., 1989. Enhancement of Landsat Thematic Mapper imagery for residual soil mapping in SW Minas Gerais State, Brazil: a prospecting case history in greenstone belt terrain. In: Seventh Thematic Conference on Remote Sensing for Exploration Geology, Calgary, Alberta, Canada: Erim.

Crosta, A.P., Sabine, C., Taranik, J.V., 1998. Hydrothermal alteration mapping at Bodie, California, using AVIRIS hyperspectral data. Remote Sensing of Environment 65, 309–319.

Cudahy, T., Hewson, R., 2002. ASTER geological case histories: porphyry-skarn-epithermal, iron oxide Cu-Au and Broken hill Pb-Zn-Ag. In: Annual General Meeting of the Geological Remote Sensing Group 'ASTER Unveiled', Burlington House, Piccadilly, London, UK.

Dadon, A., Ben-Dor, E., Beyth, M., Karnieli, A., 2011. Examination of spaceborne imaging spectroscopy data utility for stratigraphic and lithologic mapping. Journal of Applied Remote Sensing, 5.

Debba, P., Carranza, E.J.M., Stein, A., van der Meer, F.D., 2009. Deriving optimal exploration target zones on mineral prospectivity maps. Mathematical Geosciences 41, 421–446.

Dennison, P.E., Roberts, D.A., 2003. Endmember selection for multiple endmember spectral mixture analysis using endmember average RMSE. Remote Sensing of Environment 87, 123–135.

Drury, S.A., 1987. Image Interpretation in Geology. Allen & Unwin, Boston.

Duke, E.F., 1994. Near-infrared spectra of muscovite, Tschermak substitution, and metamorphic reaction progress—implications for remote-sensing. Geology 22, 621–624.

Duke, E.F., Lewis, R.S., 2010. Near infrared spectra of white mica in the Belt Supergroup and implications for metamorphism. American Mineralogist 95, 908–920.

Ehlmann, B.L., Mustard, J.F., Swayze, G.A., Clark, R.N., Bishop, J.L., Poulet, F., Marais, D.J.D., Roach, L.H., Milliken, R.E., Wray, J.J., Barnouin-JHA, O., Murchie, S.L., 2009. Identification of hydrated silicate minerals on Mars using MRO-CRISM: geologic context near Nili Fossae and implications for aqueous alteration. Journal of Geophysical Research-Planets, 114.

Farmer, J.D., 1996. Hydrothermal systems on Mars: an assessment of present evidence. In: Bock, G.R., Goode, J.A. (Eds.), Evolution of Hydrothermal Ecosystems on Earth. John Wiley & Sons Ltd, Baffins Lane, Chichester, West Sussex, England PO19 1UD.

Ferrier, G., 1995. Evaluation of apparent surface reflectance estimation methodologies. International Journal of Remote Sensing 16, 2291–2297.

Ferrier, G., White, K., Griffiths, G., Bryant, R., Stefouli, M., 2002. The mapping of hydrothermal alteration zones on the island of Lesvos, Greece using an integrated remote sensing dataset. International Journal of Remote Sensing 23, 341–356.

Foody, G.M., Lucas, R.M., Curran, P.J., Honzak, M., 1997. Non-linear mixture modelling without end-members using an artificial neural network. International Journal of Remote Sensing 18, 937–953.

Fraser, A., Huggins, P., Rees, J., Cleverly, P., 1997. A satellite remote sensing technique for geological structure horizon mapping. International Journal of Remote Sensing 18, 1607–1615.

Gad, S., Kusky, T., 2006. Lithological mapping in the Eastern Desert of Egypt, the Barramiya area, using Landsat thematic mapper (TM). Journal of African Earth Sciences 44, 196–202.

Gad, S., Kusky, T., 2007. ASTER spectral ratioing for lithological mapping in the Arabian–Nubian shield, the neoproterozoic Wadi Kid area, Sinai, Egypt. Gondwana Research 11, 326–335.

Gaffey, S.J., 1986. Spectral reflectance of carbonate minerals in the visible and near-infrared (0.35–2.55 μ)—Calcite, aragonite, and dolomite. American Mineralogist 71, 151–162.

Gallie, E.A., Mcardle, S., Rivard, B., Francis, H., 2002. Estimating sulphide ore grade in broken rock using visible/infrared hyperspectral reflectance spectra. International Journal of Remote Sensing 23, 2229–2246.

Gendrin, A., Mangold, N., Bibring, J.P., Langevin, Y., Gondet, B., Poulet, F., Bonello, G., Quantin, C., Mustard, J., Arvidson, R., Lemouelic, S., 2005. Suffates in martian layered terrains: the OMEGA/Mars Express view. Science 307, 1587–1591.

Gersman, R., Ben-Dor, E., Beyth, M., Avigad, D., Abraha, M., Kibreab, A., 2008. Mapping of hydrothermally altered rocks by the EO-1 Hyperion sensor, Northern Danakil Depression, Eritrea. International Journal of Remote Sensing 29, 3911–3936.

Gillespie, A., Kahle, A., Walker, R.E., 1987. Color enhancement of highly correlated images. II. Channel ratio and chromaticity transformation techniques. Remote Sensing of Environment 22, 343–365.

Glasser, C., Groth, D., Frauendorf, J., 2011. Monitoring of hydrochemical parameters of lignite mining lakes in Central Germany using airborne hyperspectral casi-scanner data. International Journal of Coal Geology 86, 40–53.

Goetz, A.F.H., 2009. Three decades of hyperspectral remote sensing of the Earth: a personal view. Remote Sensing of Environment 113, S5–S16.

Goetz, A.F.H., Rowan, L.C., 1981. Geologic remote-sensing. Science 211, 781–791.

Gomez, C., Delacourt, C., Allemand, P., Ledru, P., Wackerle, R., 2005. Using ASTER remote sensing data set for geological mapping, in Namibia. Physics and Chemistry of the Earth 30, 97–108.

Guanter, L., Richter, R., Kaufmann, H., 2009a. On the application of the MODTRAN4 atmospheric radiative transfer code to optical remote sensing. International Journal of Remote Sensing 30, 1407–1424.

Guanter, L., Segl, K., Kaufmann, H., 2009b. Simulation of optical remote-sensing scenes with application to the EnMAP hyperspectral mission. IEEE Transactions on Geoscience and Remote Sensing 47, 2340–2351.

Gupta, R.P., 2003. Remote Sensing Geology. Springer-Verlag Berlin, Heidelberg, Germany.

Harris, J.R., Rogge, D., Hitchcock, R., Ijewliw, O., Wright, D., 2005. Mapping lithology in Canada's Arctic: application of hyperspectral data using the minimum noise fraction transformation and matched filtering. Canadian Journal of Earth Sciences 42, 2173–2193.

Harsanyi, J.C., Chang, C.I., 1994. Hyperspectral image classification and dimensionality reduction—an orthogonal subspace projection approach. IEEE Transactions on Geoscience and Remote Sensing 32, 779–785.

Haselwimmer, C.E., Riley, T.R., Liu, J.G., 2011. Lithologic mapping in the Oscar II Coast area, Graham Land, Antarctic Peninsula using ASTER data. International Journal of Remote Sensing 32, 2013–2035.

Hecker, C., van der Meijde, M., van der Werff, H., van der Meer, F.D., 2008. Assessing the influence of reference spectra on synthetic SAM classification results. IEEE Transactions on Geoscience and Remote Sensing 46, 4162–4172.

Hecker, C., van der Meijde, M., van der Meer, F.D., 2010. Thermal infrared spectroscopy on feldspars—successes, limitations and their implications for remote sensing. Earth-Science Reviews 103, 60–70.

Hellman, M.J., Ramsey, M.S., 2004. Analysis of hot springs and associated deposits in Yellowstone National Park using ASTER and AVIRIS remote sensing. Journal of Volcanology and Geothermal Research 135, 195–219.

Hewson, R.D., Cudahy, T.J., Mizuhiko, S., Ueda, K., Mauger, A.J., 2005. Seamless geological map generation using ASTER in the Broken Hill-Curnamona province of Australia. Remote Sensing of Environment 99, 159–172.

Hook, S.J., Kahle, A.B., 1996. The micro Fourier Transform Interferometer (mu FTIR)—a new field spectrometer for acquisition of infrared data of natural surfaces. Remote Sensing of Environment 56, 172–181.

Hook, S.J., Gabell, A.R., Green, A.A., Kealy, P.S., 1992. A comparison of techniques for extracting emissivity information from thermal infrared data for geologic studies. Remote Sensing of Environment 42, 123–135.

Hook, S.J., Cudahy, T.J., Kahle, A.B., Whitbourn, L.B., 1998. Synergy of active and passive airborne thermal infrared systems for surface compositional mapping. Journal of Geophysical Research—Solid Earth 103, 18269–18276.

Hook, S.J., Karlstrom, K.E., Miller, C.F., Mccaffrey, K.J.W., 1994. Mapping the Piute mountains, California, with thermal infrared multispectral scanner (TIMS) images. Journal of Geophysical Research-Solid Earth 99, 15605–15622.

Horig, B., Kuhn, F., Oschutz, F., Lehmann, F., 2001. HyMap hyperspectral remote sensing to detect hydrocarbons. International Journal of Remote Sensing 22, 1413–1422.

Hubbard, B.E., Crowley, J.K., Zimbelman, D.R., 2003. Comparative alteration mineral mapping using visible to shortwave infrared (0.4–2.4 μm) Hyperion, ALI, and ASTER imagery. IEEE Transactions on Geoscience and Remote Sensing 41, 1401–1410.

Hunt, G.R., 1977. Spectral signatures of particulate minerals in the visible and near-infrared. Geophysics 42, 501–513.

Huntington, J.F., 1996. The role of remote sensing in finding hydrothermal mineral deposits on Earth. In: Bock, G.R., Goode, J.A. (Eds.), Evolution of Hydrothermal Ecosystems on Earth.

Kalelioglu, O., Zorlu, K., Kurt, M.A., Gul, M., Guler, C., 2009. Delineating compositionally different dykes in the Uluksla basin (Central Anatolia, Turkey) using computer-enhanced multi-spectral remote sensing data. International Journal of Remote Sensing 30, 2997–3011.

Kavak, K.S., 2005. Recognition of gypsum geohorizons in the Sivas Basin (Turkey) using ASTER and Landsat ETM+ images. International Journal of Remote Sensing 26, 4583–4596.

Kavak, K.S., Inan, S., 2002. Enhancement facilities of SPOT XS imagery in remote sensing geology: an example from the Sivas Tertiary Basin (central Anatolia/Turkey). International Journal of Remote Sensing 23, 701–710.

Kawashima, T., Narimatsu, Y., Inada, H., Ishida, J., Hamada, K., Ito, Y., Yoshida, J., Ohgi, N., Tatsumi, K., Harada, H., Kawanishi, T., Sakuma, F., Iwasaki, A., 2010. The functional evaluation model for the on-board hyperspectral radiometer. In: Larar, A.M., Chung, H.S., Suzuki, M. (Eds.), Multispectral, Hyperspectral, and Ultraspectral Remote Sensing Technology, Techniques, and Applications III. Spie—International Society for Optical Engineering, Bellingham.

Kaya, S., Muftuoglu, O., Tuysuz, O., 2004. Tracing the geometry of an active fault using remote sensing and digital elevation model: Ganos segment, North Anatolian Fault zone, Turkey. International Journal of Remote Sensing 25, 3843–3855.

Kettles, I.M., Rencz, A.N., Bauke, S.D., 2000. Integrating landsat, geologic, and airborne gamma ray data as an aid to surficial geology mapping and mineral exploration in the Manitouwadge area, Ontario. Photogrammetric Engineering and Remote Sensing 66, 437–445.

Khan, S.D., Mahmood, K., Casey, J.F., 2007. Mapping of Muslim Bagh ophiolite complex (Pakistan) using new remote sensing, and field data. Journal of Asian Earth Sciences 30, 333–343.

Kirkland, L., Herr, K., Keim, E., Adams, P., Salisbury, J., Hackwell, J., Treiman, A., 2002. First use of an airborne thermal infrared hyperspectral scanner for compositional mapping. Remote Sensing of Environment 80, 447–459.

Kohler, D.D.R., Bissett, W.P., Steward, R.G., Davis, C.O., 2004. New approach for the radiometric calibration of spectral imaging systems. Optics Express 12, 2463–2477.

Kozak, P.K., Duke, E.F., Roselle, G.T., 2004. Mineral distribution in contact-metamorphosed siliceous dolomite at Ubehebe Peak, California, based on airborne imaging spectrometer data. American Mineralogist 89, 701–713.

Kratt, C., Calvin, W.M., Coolbaugh, M.F., 2010. Mineral mapping in the Pyramid Lake basin: hydrothermal alteration, chemical precipitates and geothermal energy potential. Remote Sensing of Environment 114, 2297–2304.

Kruger, G., Erzinger, J., Kaufmann, H., 1998. Laboratory and airborne reflectance spectroscopic analyses of lignite overburden dumps. Journal of Geochemical Exploration 64, 47–65.

Kruse, F.A., 1996. Identification and mapping of minerals in drill core using hyperspectral image analysis of infrared reflectance spectra. International Journal of Remote Sensing 17, 1623–1632.

Kruse, F.A., Lefkoff, A.B., Boardman, J.W., Heidebrecht, K.B., Shapiro, A.T., Barloon, P.J., Goetz, A.F.H., 1993. The spectral image-processing system (SIPS)—interactive visualisation and analysis of imaging spectrometer data. Remote Sensing of Environment 44, 145–163.

Kruse, F.A., Boardman, J.W., Huntington, J.F., 2003. Comparison of airborne hyperspectral data and EO-1 Hyperion for mineral mapping. IEEE Transactions on Geoscience and Remote Sensing 41, 1388–1400.

Kruse, F.A., Perry, S.L., Caballero, A., 2006. District-level mineral survey using airborne hyperspectral data, Los Menucos, Argentina. Annals of Geophysics 49, 83–92.

Kuhn, F., Oppermann, K., Horig, B., 2004. Hydrocarbon index—an algorithm for hyperspectral detection of hydrocarbons. International Journal of Remote Sensing 25, 2467–2473.

Launeau, P., Girardeau, J., Sotin, C., Tubia, J.M., 2004. Comparison between field measurements and airborne visible and infrared mapping spectrometry (AVIRIS and HyMap) of the Ronda peridotite massif (south-west Spain). International Journal of Remote Sensing 25, 2773–2792.

Lee, S., Talib, J.A., 2005. Probabilistic landslide susceptibility and factor effect analysis. Environmental Geology 47, 982–990.

Leprince, S., Barbot, S., Ayoub, F., Avouac, J.P., 2007. Automatic and precise orthorectification, coregistration, and subpixel correlation of satellite images, application to ground deformation measurements. IEEE Transactions on Geoscience and Remote Sensing 45, 1529–1558.

Li, P.J., Long, X.Y., Liu, L., 2007. Ophiolite mapping using ASTER data: a case study of Derni ophiolite complex. Acta Petrologica Sinica 23, 1175–1180.

Loizeau, D., Mangold, N., Poulet, F., Bibring, J.P., Gendrin, A., Ansan, V., Gomez, C., Gondet, B., Langevin, Y., Masson, P., Neukum, G., 2007. Phyllosilicates in the Mawrth Vallis region of Mars. Journal of Geophysical Research—Planets, 112.

Loughlin, W.P., 1991. Principal component analysis for alteration mapping. Photogrammetric Engineering and Remote Sensing 57, 1163–1169.

Lyder, D., Feng, J., Rivard, B., Gallie, A., Cloutis, E., 2010. Remote bitumen content estimation of Athabasca oil sand from hyperspectral infrared reflectance spectra using Gaussian singlets and derivative of Gaussian wavelets. Fuel 89, 760–767.

Macdonald, I.R., Guinasso, N.L., Ackleson, S.G., Amos, J.F., Duckworth, R., Sassen, R., Brooks, J.M., 1993. Natural oil-slicks in the Gulf-of-Mexico visible from space. Journal of Geophysical Research—Oceans 98, 16351–16364.

Madani, A.A., Emam, A.A., 2011. SWIR ASTER band ratios for lithological mapping and mineral exploration: a case study from El Hudi area, southeastern desert, Egypt. Arabian Journal of Geosciences 4, 45–52.

Mangold, N., Gendrin, A., Gondet, B., Lemouelic, S., Quantin, C., Ansan, V., Bibring, J.P., Langevin, Y., Masson, P., Neukum, G., 2008. Spectral and geological study of the sulfate-rich region of West Candor Chasma, Mars. Icarus 194, 519–543.

Mars, J.C., Crowley, J.K., 2003. Mapping mine wastes and analyzing areas affected by selenium-rich water runoff in southeast Idaho using AVIRIS imagery and digital elevation data. Remote Sensing of Environment 84, 422–436.

Mars, J.C., Rowan, L.C., 2006. Regional mapping of phyllic- and argillic-altered rocks in the Zagros magmatic arc, Iran, using Advanced Spaceborne Thermal Emission and Reflection Radiometer (ASTER) data and logical operator algorithms. Geosphere 2, 161–186.

Mars, J.C., Rowan, L.C., 2010. Spectral assessment of new ASTER SWIR surface reflectance data products for spectroscopic mapping of rocks and minerals. Remote Sensing of Environment 114, 2011–2025.

Mars, J.C., Rowan, L.C., 2011. ASTER spectral analysis and lithologic mapping of the Khanneshin carbonatite volcano, Afghanistan. Geosphere 7, 276–289.

Martinez, P.J., Perez, R.M., Plaza, A., Aguilar, P.L., Cantero, M.C., Plaza, J., 2006. Endmember extraction algorithms from hyperspectral images. Annals of Geophysics 49, 93–101.

Massironi, M., Bertoldi, L., Calafa, P., Visona, D., Bistacchi, A., Giardino, C., Schiavo, A., 2008. Interpretation and processing of ASTER data for geological mapping and granitoids detection in the Saghro massif (eastern Anti-Atlas, Morocco). Geosphere 4, 736–759.

Mountrakis, G., Im, J., Ogole, C., 2011. Support vector machines in remote sensing: a review. Isprs Journal of Photogrammetry and Remote Sensing 66, 247–259.

Mumby, P.J., Green, E.P., Edwards, A.J., Clark, C.D., 1997. Coral reef habitat-mapping: how much detail can remote sensing provide? Marine Biology 130, 193–202.

Murchie, S., Arvidson, R., Bedini, P., Beisser, K., Bibring, J.P., Bishop, J., Boldt, J., Cavender, P., Choo, T., Clancy, R.T., Darlington, E.H., Marais, D.D., Espiritu, R., Fort, D., Green, R., Guinness, E., Hayes, J., Hash, C., Heffernan, K., Hemmler, J., Heyler, G., Humm, D., Hutcheson, J., Izenberg, N., Lee, R., Lees, J., Lohr, D., Malaret, E., Martin, T., Mcgovern, J.A., Mcguire, P., MORRIS, R., Mustard, J., Pelkey, S., Rhodes, E., Robinson, M., Roush, T., Schaefer, E., Seagrave, G., Seelos, F., Silverglate, P., Slavney, S., Smith, M., Shyong, W.J., Strohbehn, K., taylor, H., THOMPSON, P., Tossman, B., Wirzburger, M., Wolff, M., 2007. Compact reconnaissance Imaging Spectrometer for Mars (CRISM) on Mars Reconnaissance Orbiter (MRO). Journal of Geophysical Research-Planets, 112.

Mustard, J.F., Poulet, F., Gendrin, A., Bibring, J.P., Langevin, Y., Gondet, B., Mangold, N., Bellucci, G., Altieri, F., 2005. Olivine and pyroxene, diversity in the crust of Mars. Science 307, 1594–1597.

Mustard, J.F., Murchie, S.L., Pelkey, S.M., Ehlmann, B.L., Milliken, R.E., Grant, J.A., Bibring, J.P., Poulet, F., Bishop, J., Dobrea, E.N., Roach, L., Seelos, F., Arvidson, R.E., Wiseman, S., Green, R., Hash, C., Humm, D., Malaret, E., Mcgovern, J.A., Seelos, K., Clancy, T., Clark, R., des Marais, D., Izenberg, N., Knudson, A., Langevin, Y., Martin, T., Mcguire, P., Morris, R., Robinson, M., Roush, T., Smith, M., Swayze, G., Taylor, H., Titus, T., Wolff, M., 2008. Hydrated silicate minerals on mars observed by the Mars reconnaissance orbiter CRISM instrument. Nature 454, 305–309.

Nielsen, A.A., 2001. Spectral mixture analysis: linear and semi-parametric full and iterated partial unmixing in multi- and hyperspectral image data. International Journal of Computer Vision 42, 17–37.

Oppenheimer, C., Francis, P.W., Rothery, D.A., Carlton, R.W.T., Glaze, L.S., 1993. Infrared image-analysis of volcanic thermal features—Lascar volcano, Chili, 1984–1992. Journal of Geophysical Research—Solid Earth 98, 4269–4286.

Oztan, N.S., Suzen, M.L., 2011. Mapping evaporate minerals by ASTER. International Journal of Remote Sensing 32, 1651–1673.

Pearlman, J.S., Barry, P.S., Segal, C.C., Shepanski, J., Beiso, D., Carman, S.L., 2003. Hyperion, a space-based imaging spectrometer. IEEE Transactions on Geoscience and Remote Sensing 41, 1160–1173.

Pelkey, S.M., Mustard, J.F., Murchie, S., Clancy, R.T., Wolff, M., Smith, M., Milliken, R., Bibring, J.P., Gendrin, A., Poulet, F., Langevin, Y., Gondet, B., 2007. CRISM multispectral summary products: parameterizing mineral diversity on Mars from reflectance. Journal of Geophysical Research—Planets, 112.

Pena, S.A., Abdelsalam, M.G., 2006. Orbital remote sensing for geological mapping in southern Tunisia: implication for oil and gas exploration. Journal of African Earth Sciences 44, 203–219.

Plaza, A., Martinez, P., Perez, R., Plaza, J., 2004. A quantitative and comparative analysis of endmember extraction algorithms from hyperspectral data. IEEE Transactions on Geoscience and Remote Sensing 42, 650–663.

Pohl, C., van Genderen, J.L., 1998. Multisensor image fusion in remote sensing: concepts, methods and applications. International Journal of Remote Sensing 19, 823–854.

Poulet, F., Bibring, J.P., Mustard, J.F., Gendrin, A., Mangold, N., Langevin, Y., Arvidson, R.E., Gondet, B., Gomez, C., Omega, T., 2005. Phyllosilicates on Mars and implications for early martian climate. Nature 438, 623–627.

Prinz, T., 1996. Multispectral remote sensing of the Gosses Bluff impact crater, central Australia (NT) by using Landsat-TM and ERS-1 data. Isprs Journal of Photogrammetry and Remote Sensing 51, 137–149.

Qari, M.H.T., Madani, A.A., Matsah, M.I.M., Hamimi, Z., 2008. Utilization of ASTER and Landsat data in geologic mapping of basement rocks of Arafat Area, Saudi Arabia. Arabian Journal for Science and Engineering 33, 99–116.

Qiu, F., Abdelsalam, M., Thakkar, P., 2006. Spectral analysis of ASTER data covering part of the Neoproterozoic Allaqi-Heiani suture, Southern Egypt. Journal of African Earth Sciences 44, 169–180.

Ragona, D., Minster, B., Rockwell, T., Jussila, J., 2006. Field imaging spectroscopy: a new methodology to assist the description, interpretation, and archiving of paleoseismological information from faulted exposures. Journal of Geophysical Research-Solid Earth, 111.

Rajendran, S., Thirunavukkarasu, A., Balamurugan, G., Shankar, K., 2011. Discrimination of iron ore deposits of granulite terrain of Southern Peninsular India using ASTER data. Journal of Asian Earth Sciences 41, 99–106.

Rajesh, H.M., 2004. Application of remote sensing and GIS in mineral resource mapping—an overview. Journal of Mineralogical and Petrological Sciences 99, 83–103.

Ranjbar, H., Honarmand, M., Moezifar, Z., 2004. Application of the Crosta technique for porphyry copper alteration mapping, using ETM+ data in the southern part of the Iranian volcanic sedimentary belt. Journal of Asian Earth Sciences 24, 237–243.

Riaza, A., Muller, A., 2010. Hyperspectral remote sensing monitoring of pyrite mine wastes: a record of climate variability (Pyrite Belt, Spain). Environmental Earth Sciences 61, 575–594.

Richter, R., 1996. Atmospheric correction of DAIS hyperspectral image data. Computers & Geosciences 22, 785–793.

Richter, R., Schlapfer, D., 2002. Geo-atmospheric processing of airborne imaging spectrometry data. Part 2: atmospheric/topographic correction. International Journal of Remote Sensing 23, 2631–2649.

Richter, R., Muller, A., Heiden, U., 2002. Aspects of operational atmospheric correction of hyperspectral imagery. International Journal of Remote Sensing 23, 145–157.

Richter, N., Staenz, K., Kaufmann, H., 2008. Spectral unmixing of airborne hyperspectral data for baseline mapping of mine tailings areas. International Journal of Remote Sensing 29, 3937–3956.

Rigol, J.P., Chica-Olmo, M., 1998. Merging remote-sensing images for geological-environmental mapping: application to the Cabo de Gata-Nijar Natural Park, Spain. Environmental Geology 34, 194–202.

Rivard, B., Zhang, J., Feng, J., Sanchez-Azofeifa, G.A., 2009. Remote predictive lithologic mapping in the Abitibi Greenstone Belt, Canada, using airborne hyperspectral imagery. Canadian Journal of Remote Sensing 35, S95–S105.

Rockwell, B.W., Hofstra, A.H., 2008. Identification of quartz and carbonate minerals across northern Nevada using ASTER thermal infrared emissivity data—implications for geologic mapping and mineral resource investigations in well-studied and frontier areas. Geosphere 4, 218–246.

Rowan, L.C., Mars, J.C., 2003. Lithologic mapping in the Mountain Pass, California area using Advanced Spaceborne Thermal Emission and Reflection Radiometer (ASTER) data. Remote Sensing of Environment 84, 350–366.

Rowan, L.C., Crowley, J.K., Schmidt, R.G., Ager, C.M., Mars, J.C., 2000. Mapping hydrothermally altered rocks by analyzing hyperspectral image (AVLRIS) data of forested areas in the Southeastern United States. Journal of Geochemical Exploration 68, 145–166.

Roy, R., Launeau, P., Carrere, V., Pinet, P., Ceuleneer, G., Clenet, H., Daydou, Y., Girardeau, J., Amri, I., 2009. Geological mapping strategy using visible near-infrared-shortwave infrared hyperspectral remote sensing: Application to the Oman ophiolite (Sumail Massif). Geochemistry Geophysics Geosystems, 10.

Rytuba, J.J., Arribas, A., Cunningham, C.G., Mckee, E.H., Podwysocki, M.H., Smith, J.G., Kelly, W.C., 1990. Mineralized and unmineralized calderas in Spain. 2. Evolution of the Rodalquilar caldera complex and associated gold-alunite deposits. Mineralium Deposita 25, S29–S35.

Sabins, F.F., 1996. Remote Sensing: Principles and Interpretation. Worth publishers, New York.

Sabins, F.F., 1999. Remote sensing for mineral exploration. Ore Geology Reviews 14, 157–183.

Salisbury, J.W., Daria, D.M., 1992. Emissivity of terrestrial materials in the 8-14 MU-M atmospheric window. Remote Sensing of Environment 42, 83–106.

Salisbury, J.W., Daria, D.M., 1994. Emissivity of terrestrial materials in the 3-5-MU-M atmospheric window. Remote Sensing of Environment 47, 345–361.

Salisbury, J.W., Walter, L.S., 1989. Thermal infrared (2.5–13.5 MU-M) spectroscopic remote sensing of igneous rock types on particulate planetary surfaces. Journal of Geophysical Research—Solid Earth and Planets 94, 9192–9202.

Salisbury, J.W., Walter, L.S., Vergo, N., 1989. Availability of a library of infrared (2.1–25.0 MU-M) mineral spectra. American Mineralogist 74, 938–939.

Schaepman, M.E., Ustin, S.L., Plaza, A.J., Painter, T.H., Verrelst, J., Liang, S.L., 2009. Earth system science related imaging spectroscopy—an assessment. Remote Sensing of Environment 113, S123–S137.
Scheidt, S., Lancaster, N., Ramsey, M., 2011. Eolian dynamics and sediment mixing in the Gran Desierto, Mexico, determined from thermal infrared spectroscopy and remote-sensing data. Geological Society of America Bulletin 123, 1628–1644.
Schetselaar, E.M., Chung, C.J.F., Kim, K.E., 2000. Integration of Landsat TM, gamma-ray, magnetic, and field data to discriminate lithological units in vegetated granite-gneiss terrain. Remote Sensing of Environment 71, 89–105.
Schroeter, L., Glasser, C., 2011. Analyses and monitoring of lignite mining lakes in Eastern Germany with spectral signatures of Landsat TM satellite data. International Journal of Coal Geology 86, 27–39.
Segl, K., Guanter, L., Kaufmann, H., Schubert, J., Kaiser, S., Sang, B., Hofer, S., 2010. Simulation of spatial sensor characteristics in the context of the EnMAP hyperspectral mission. IEEE Transactions on Geoscience and Remote Sensing 48, 3046–3054.
Settle, J.J., Drake, N.A., 1993. Linear mixing and the estimation of ground cover proportions. International Journal of Remote Sensing 14, 1159–1177.
Shang, J.L., Morris, B., Howarth, P., Levesque, J., Staenz, K., Neville, B., 2009. Mapping mine tailing surface mineralogy using hyperspectral remote sensing. Canadian Journal of Remote Sensing 35, S126–S141.
Shimabukuro, Y.E., Smith, J.A., 1991. The least-squares mixing models to generate fraction images derived from remote-sensing mutispectral data. IEEE Transactions on Geoscience and Remote Sensing 29, 16–20.
Sillitoe, R.H., 1996. Granites and metal deposits. Episodes 19, 126–133.
Sillitoe, R.H., 2010. Porphyry copper systems. Economic Geology 105, 3–41.
Singhroy, V., Mattar, K.E., Gray, A.L., 1998. Landslide characterisation in Canada using interferometric SAR and combined SAR and TM images. In: Susskind, J., Singhroy, V., Tanaka, S. (Eds.), Remote Sensing: Inversion Problems and Natural Hazards.
Stuffler, T., Kaufmann, C., Hofer, S., Forster, K.P., Schreier, G., Mueller, A., Eckardt, A., Bach, H., Penne, B., Benz, U., Haydn, R., 2007. The EnMAP hyperspectral imager—an advanced optical payload for future applications in Earth observation programmes. Acta Astronautica 61, 115–120.
Swayze, G.A., Kokaly, R.F., Higgins, C.T., Clinkenbeard, J.P., Clark, R.N., Lowers, H.A., Sutley, S.J., 2009. Mapping potentially asbestos-bearing rocks using imaging spectroscopy. Geology 37, 763–766.
Tangestani, M.H., Moore, F., 2001. Comparison of three principal component analysis techniques to porphyry copper alteration mapping: a case study, Meiduk area, Kerman, Iran. Canadian Journal of Remote Sensing 27, 176–182.
Tompkins, S., Mustard, J.F., Pieters, C.M., Forsyth, D.W., 1997. Optimization of endmembers for spectral mixture analysis. Remote Sensing of Environment 59, 472–489.
van der Meer, F., 1996. Classification of remotely-sensed imagery using an indicator kriging approach: application to the problem of calcite–dolomite mineral mapping. International Journal of Remote Sensing 17, 1233–1249.
van der Meer, F., 1997. What does multisensor image fusion add in terms of information content for visual interpretation? International Journal of Remote Sensing 18, 445–452.
van der Meer, F., 1999. Iterative spectral unmixing (ISU). International Journal of Remote Sensing 20, 3431–3436.
van der Meer, F., 2006a. The effectiveness of spectral similarity measures for the analysis of hyperspectral imagery. International Journal of Applied Earth Observation and Geoinformation 8, 3–17.
van der Meer, F., 2006b. Indicator kriging applied to absorption band analysis in hyperspectral imagery: a case study from the Rodalquilar epithermal gold mining area, SE Spain. International Journal of Applied Earth Observation and Geoinformation 8, 61–72.
van der Meer, F., Bakker, W., 1997. Cross correlogram spectral matching: application to surface mineralogical mapping by using AVIRIS data from Cuprite, Nevada. Remote Sensing of Environment 61, 371–382.
van der Meer, F., van Dijk, P., van der Werff, H., Yang, H., 2002. Remote sensing and petroleum seepage: a review and case study. Terra Nova 14, 1–17.
van der Meer, F., van der Werff, H., de Jong, S., 2009. Pre-processing of optical imagery. In: Warner, T., Nellis, M.D., Foody, G.M. (Eds.), The SAGE Handbook of Remote Sensing. SAGE Publishers, London, UK.
van der Werff, H.M.A., Bakker, W.H., van der Meer, F.D., Siderius, W., 2006. Combining spectral signals and spatial patterns using multiple Hough transforms: an application for detection of natural gas seepages. Computers & Geosciences 32, 1334–1343.
van Ruitenbeek, F.J.A., Cudahy, T., Hale, M., van der Meer, F.D., 2005. Tracing fluid pathways in fossil hydrothermal systems with near-infrared spectroscopy. Geology 33, 597–600.
van Ruitenbeek, F.J.A., Debba, P., van der Meer, F.D., cudahy, T., van der Meijde, M., Hale, M., 2006. Mapping white micas and their absorption wavelengths using hyperspectral band ratios. Remote Sensing of Environment 102, 211–222.
Vane, G., Goetz, A.F.H., 1988. Terrestrial imaging spectroscopy. Remote Sensing of Environment 24, 1–29.
Vane, G., Goetz, A.F.H., 1993. Terrestrial imaging spectrometry—current status, future-trends. Remote Sensing of Environment 44, 117–126.
Vane, G., Green, R.O., Chrien, T.G., Enmark, H.T., Hansen, E.G., Porter, W.M., 1993. The Airborne Visible Infrared Imaging Spectrometer (AVIRIS). Remote Sensing of Environment 44, 127–143.
Vaughan, R.G., Calvin, W.M., Taranik, J.V., 2003. SEBASS hyperspectral thermal infrared data: surface emissivity measurement and mineral mapping. Remote Sensing of Environment 85, 48–63.
Vaughan, R.G., Hook, S.J., Calvin, W.M., Taranik, J.V., 2005. Surface mineral mapping at Steamboat Springs, Nevada, USA, with multi-wavelength thermal infrared images. Remote Sensing of Environment 99, 140–158.
Wang, A., Freeman, J.J., Jolliff, B.L., Chou, I.M., 2006. Sulfates on Mars: a systematic Raman spectroscopic study of hydration states of magnesium sulfates. Geochimica Et Cosmochimica Acta 70, 6118–6135.
Watanabe, H., 2002. Rock type classification by multi-band TIR of ASTER. In: Annual General Meeting of the Geological Remote Sensing Group 'ASTER Unveiled', Burlington House, Piccadilly, London, UK.
Watts, D.R., Harris, N.B.W., Grp, N.G.S.W., 2005. Mapping granite and gneiss in domes along the North Himalayan antiform with ASTER SWIR band ratios. Geological Society of America Bulletin 117, 879–886.
Windeler, D.S., 1993. Garnet-pyroxene alteration mapping in the Ludwig Skarn (Yerington, Nevada) with Geoscan airborne multispectral data. Photogrammetric Engineering and Remote Sensing 59, 1277–1286.
Windeler, D.S., Lyon, R.J.P., 1991. Discriminating dolomitization of marble in the Ludwig Skarn near Yerington, Nevada using high-resolution airborne infrared imagery. Photogrammetric Engineering and Remote Sensing 57, 1171–1177.
Xu, N., Hu, Y.X., Lei, B., Hong, Y.T., Dang, F.X., 2011. Mineral information extraction for hyperspectral image based on modified spectral feature fitting algorithm. Spectroscopy and Spectral Analysis 31, 1639–1643.
Yamaguchi, Y., Naito, C., 2003. Spectral indices for lithologic discrimination and mapping by using the ASTER SWIR bands. International Journal of Remote Sensing 24, 4311–4323.
Yamaguchi, Y., Kahle, A.B., Tsu, H., Kawakami, T., Pniel, M., 1998. Overview of Advanced Spaceborne Thermal Emission and Reflection Radiometer (ASTER). IEEE Transactions on Geoscience and Remote Sensing 36, 1062–1071.
Yang, K., Huntington, J.F., Browne, P.R.L., Ma, C., 2000. An infrared spectral reflectance study of hydrothermal alteration minerals from the Te Mihi sector of the Wairakei geothermal system, New Zealand. Geothermics 29, 377–392.
Yang, K., Browne, P.R.L., Huntington, J.F., Walshe, J.L., 2001. Characterising the hydrothermal alteration of the Broadlands-Ohaaki geothermal system, New Zealand, using short-wave infrared spectroscopy. Journal of Volcanology and Geothermal Research 106, 53–65.
Yesou, H., Besnus, Y., Rolet, J., 1993. Extraction of spectral information from Landsat-TM data and merger with SPOT panchromatic imagery - a contribution to the study of geological structures. Isprs Journal of Photogrammetry and Remote Sensing 48, 23–36.
Zhang, X., Pamer, M., Duke, N., 2007. Lithologic and mineral information extraction for gold exploration using ASTER data in the south Chocolate Mountains (California). Isprs Journal of Photogrammetry and Remote Sensing 62, 271–282.
Zortea, M., Plaza, A., 2009. Spatial preprocessing for endmember extraction. IEEE Transactions on Geoscience and Remote Sensing 47, 2679–2693.